

# Lower oceanic $\delta^{13}\text{C}$ during the Last Interglacial Period compared to the Holocene

Shannon A. Bengtson<sup>1,2</sup>, Laurie C. Men viel<sup>1</sup>, Katrin J. Meissner<sup>1,2</sup>, Lise Missiaen<sup>1</sup>, Carlye D. Peterson<sup>3</sup>, Lorraine E. Lisiecki<sup>4</sup>, and Fortunat Joos<sup>5,6</sup>

<sup>1</sup>Climate Change Research Centre, The University of New South Wales, Sydney, Australia

<sup>2</sup>The Australian Research Council Centre of Excellence for Climate Extremes, Australia

<sup>3</sup>Earth Sciences, University of California, Riverside, California, USA

<sup>4</sup>Department of Earth Science, University of California, Santa Barbara, California, USA

<sup>5</sup>Climate and Environmental Physics, Physics Institute, University of Bern, Bern, Switzerland

<sup>6</sup>Oeschger Centre for Climate Change Research, University of Bern, Bern, Switzerland

**Correspondence:** Shannon A. Bengtson (s.bengtson@unsw.edu.au)

## Abstract.

The last time in Earth's history when high latitudes were warmer than during pre-industrial times was the last interglacial period (LIG, 129–116 ka BP). Since the LIG is the most recent and best documented interglacial, it can provide insights into climate processes in a warmer world. However, some key features of the LIG are not well constrained, notably the oceanic circulation and the global carbon cycle. Here, we use a new database of LIG benthic  $\delta^{13}\text{C}$  to investigate these two aspects. We find that the oceanic mean  $\delta^{13}\text{C}$  was  $\sim 0.2\text{‰}$  lower during the LIG (here defined as 125–120 ka BP) when compared to the Holocene (7–2 ka BP). A lower terrestrial carbon content at the LIG than during the Holocene could have led to both a lower oceanic  $\delta^{13}\text{C}$  and atmospheric  $\delta^{13}\text{CO}_2$  as observed in paleo-records. However, given the multi-millennial timescale, the lower oceanic  $\delta^{13}\text{C}$  most likely reflects a long-term imbalance between weathering and burial of carbon. The  $\delta^{13}\text{C}$  distribution in the Atlantic Ocean suggests no significant difference in the latitudinal and depth extent of North Atlantic Deep Water (NADW) between the LIG and the Holocene. Furthermore, the data suggests that the multi-millennial mean NADW transport was similar between these two time periods.

## 1 Introduction

The most recent and well documented warm time period is the last interglacial period (LIG), which is roughly equivalent to Marine Isotope Stage (MIS) 5e (of PAGES, 2016; Shackleton, 1969). The LIG began at the end of the penultimate deglaciation and ended with the last glacial inception ( $\sim 129$ –116 thousand years before present, ka BP hereafter (Dutton and Lambeck, 2012; Govin et al., 2015; Masson-Delmotte et al., 2013; Men viel et al., 2019)). The LIG was globally warmer than pre-industrial (PI,  $\sim 1850$ –1900 (IPCC, 2013), Shackleton et al. (2020)), with PI estimated to be  $\sim 0.4\text{ }^{\circ}\text{C}$  cooler than the peak of the Holocene (10–5 ka BP) (Marcott et al., 2013). Though not an exact analogue for future warming, the LIG may still help shed light on future climates. In particular, we seek to constrain the mean LIG ocean circulation and estimate the global oceanic mean  $\delta^{13}\text{C}$ .

As greenhouse gas concentrations were comparable to the Holocene, the LIG was most likely relatively warm because of the high boreal summer insolation (Laskar et al., 2004). During the LIG, the atmospheric CO<sub>2</sub> concentration was relatively stable around ~280 p.p.m. (Bereiter et al., 2015; Lüthi et al., 2008), while during the Holocene, CO<sub>2</sub> first decreased by about 25 8 p.p.m. starting at 11.7 ka BP before increasing by ~17 p.p.m. to 277 p.p.m. at ~2 ka BP (Fig. 1a) (Köhler et al., 2017). CH<sub>4</sub> and N<sub>2</sub>O peaked at ~700 p.p.b and ~267 p.p.b, respectively, during both the LIG and the Holocene (Flückiger et al., 2002; Petit et al., 1999; Spahni et al., 2005). Global sea-level was 6–9 m higher at the LIG compared to PI (Dutton et al., 2015; Kopp et al., 2009), thus indicating significant ice-mass loss from both Antarctica and Greenland.

Strong polar warming is supported by terrestrial and marine temperature reconstructions. A global analysis of sea surface 30 temperature (SST) records suggests that the mean surface ocean was  $0.5 \pm 0.3$  °C warmer during the LIG compared to 1870–1889 (Hoffman et al., 2017), similar to another global estimate which suggests SSTs were  $0.7 \pm 0.6$  °C higher during the LIG compared to the late Holocene (McKay et al., 2011). However, there were differences in the timing of these SST peaks in different regions compared to the 1870–1889 mean: North Atlantic SSTs peaked at  $+0.6 \pm 0.5$  °C at 125 ka BP (e.g. Fig. 1b) and Southern Hemisphere extratropical SSTs peaked at  $+1.1 \pm 0.5$  °C at 129 ka BP (Hoffman et al., 2017). On land, proxy 35 records from mid to high latitudes indicate higher temperatures during the LIG compared to PI, particularly in North America (Anderson et al., 2014; Axford et al., 2011; Montero-Serrano et al., 2011). Similarly, the EPICA DOME C record suggests that the highest Antarctic temperatures from the last 800 ka occurred during the LIG (Masson-Delmotte et al., 2010) (Fig. 1c).

Polar warming was also associated with significant changes in vegetation. Pollen records suggest a contraction of tundra and 40 an expansion of boreal forests across the Arctic (CAPE, 2006), in Russia (Tarasov et al., 2005), and in North America (Govin et al., 2015; Muhs et al., 2001; de Vernal and Hillaire-Marcel, 2008). The few Saharan records suggest a green Sahara period during the LIG (Drake et al., 2011; Larrasoña et al., 2013), consistent with a stronger West African monsoon (Otto-Bliesner et al., 2020). Although these reconstructions indicate changes in vegetation distribution during the LIG, the total amount of carbon stored on land remains poorly constrained.

Recent numerical experiments of the LIG as part of the Paleoclimate Model Intercomparison Project Phase 4 (PMIP4) simulate 45 significant warming over Alaska and Siberia in boreal summer, with mean annual temperature anomalies of close to zero, which is in good agreement with the proxy record (Otto-Bliesner et al., 2020). Despite this and other recent data compilations and modelling efforts (including Bakker et al. (2013)), there are many open questions remaining about the LIG. In particular, stronger constraints are needed on the extent of Greenland and Antarctic ice sheets, on ocean circulation and the global carbon cycle, including CaCO<sub>3</sub> accumulation in shallow waters, and peat and permafrost carbon storage (Brovkin et al., 2016).

It is important to constrain the state of the Atlantic Meridional Overturning Circulation (AMOC) at the LIG given its significant role in modulating climate. Seven coupled climate models integrated with transient 130–115 ka BP boundary conditions simulate different AMOC trends, with some models producing a strengthening of the AMOC while others simulate a weakening 50 during the LIG (Bakker et al., 2013). Paleoproxy records suggest equally strong and deep North Atlantic Deep Water (NADW) during the LIG and the Holocene (e.g. Böhm et al., 2015; Lototskaya and Ganssen, 1999), with a possible southward expansion of the Arctic front related to changes in the strength of the subpolar gyre (Mokeddem et al., 2014), and AMOC

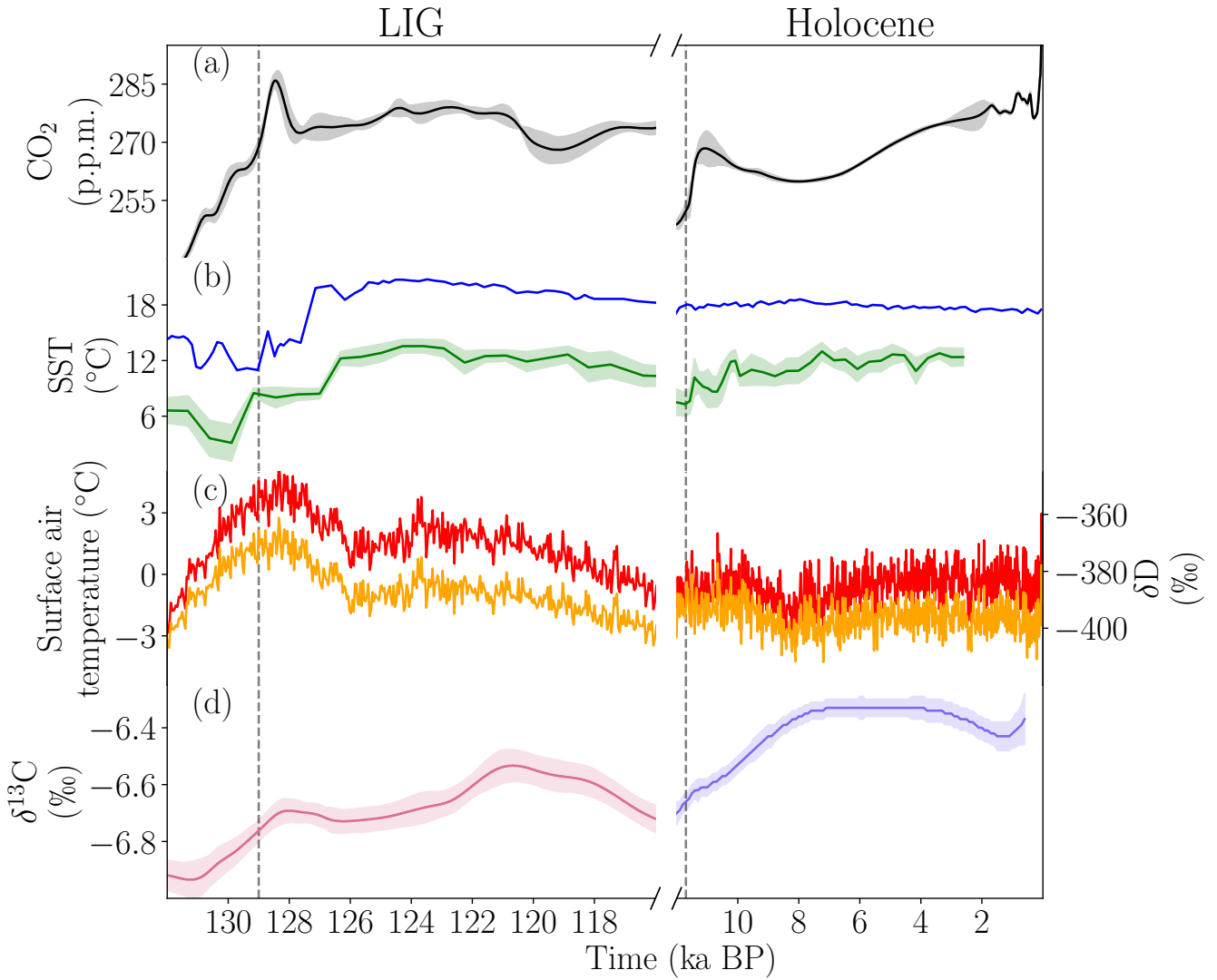


**Figure 1.** LIG and Holocene timeseries of a)  $\text{CO}_2$  stack smoothed with a spline based on the age model AICC2012 (Köhler et al., 2017), b) sea surface temperatures (SSTs) determined from alkenones and aligned with oxygen isotopes from the Iberian Margin (MD01-2444, blue, Martrat et al. (2007b)) and the North Atlantic (GIK23414-6, green, Candy and Alonso-Garcia (2018)), c) EPICA Dome C ice core (EDC96) deuterium measurements (orange) and estimated surface air temperature anomaly relative to the mean of the last 1 ka (red, Bazin et al. (2013); Jouzel et al. (2007)) on the AICC2012 time scale and d) spline of atmospheric  $\delta^{13}\text{C}$  from EPICA Dome C and the Talos Dome ice cores (Holocene, Eggleston et al. (2016)) and Monte Carlo average of three Antarctic ice cores atmospheric  $\delta^{13}\text{C}$  (LIG, Schneider et al. (2013)) both based on the age model AICC2012. Shading around the lines indicates  $1\sigma$ . Vertical grey shading indicates the periods of analysis in this paper. Grey vertical dotted lines indicate the commencement of the LIG and Holocene.

weakening during a few multi centennial-scale events between 127 and 115 ka BP (e.g. Galaasen et al., 2014b; Helmens et al., 2015; Lehman et al., 2002; Mokeddem et al., 2014; Oppo et al., 2006; Rowe et al., 2019; Tzedakis et al., 2018).

Stable carbon isotopes are a powerful tool for investigating ocean circulation (e.g. Curry and Oppo, 2005; Eide et al., 2017) and the global carbon cycle (e.g. Menzel et al., 2017; Peterson et al., 2014). Since the largest carbon isotope fractionation occurs during photosynthesis, organic matter is enriched in  $^{12}\text{C}$  (low  $\delta^{13}\text{C}$ ), while atmospheric  $\text{CO}_2$  and surface water dissolved inorganic carbon (DIC) become enriched in  $^{13}\text{C}$  (high  $\delta^{13}\text{C}$ ). Organic matter on land includes the terrestrial biosphere, as well as carbon stored in soils, such as in peats and permafrosts. Different photosynthetic pathways (which differentiate C3 and C4 plants) fractionate carbon differently, producing typical signatures of about -37 to -20 ‰ for C3 plants (Kohn, 2010) and around -13 ‰ for C4 plants (Basu et al., 2015), though these values vary with a number of factors including precipitation, atmospheric  $\text{CO}_2$  concentration and  $\delta^{13}\text{C}$ , light, nutrient availability, and plant species (Cernusak et al., 2013; Diefendorf et al., 2010; Diefendorf and Freimuth, 2017; Farquhar, 1983; Farquhar et al., 1989; Keller et al., 2017; Leavitt, 1992; Schubert and Jahren, 2012). In the ocean, phytoplankton using the C3 photosynthetic pathway are found to have fractionation during photosynthesis that depends on the concentration of dissolved  $\text{CO}_2$ . Thus, atmospheric  $\delta^{13}\text{CO}_2$  during the LIG (Fig. 1d) is influenced by the cycling of organic carbon within the ocean, changes in the amount of carbon stored in vegetation and soils, temperature-dependent air-sea flux fractionation (Lynch-Stieglitz et al., 1995; Zhang et al., 1995), and, on longer time scales, by interactions with the lithosphere (Tschumi et al., 2011). The mean surface DIC is enriched by ~8.5 ‰ compared to the atmosphere due to fractionation during air-sea gas exchange (Menzel et al., 2015; Schmittner et al., 2013).

NADW is characterised by low nutrients and high  $\delta^{13}\text{C}$  as a result of a high nutrient and carbon utilisation by marine biota and fractionation during air-sea gas exchange in the northern North Atlantic. Along its path through the Atlantic basin interior, organic matter remineralisation and mixing with southern source waters lowers  $\delta^{13}\text{C}$ , with  $\delta^{13}\text{C}$  values of ~0.5 ‰ in the deep Southern Ocean.

The tight relationship between the water masses' apparent oxygen utilisation, nutrient content and  $\delta^{13}\text{C}$  allows  $\delta^{13}\text{C}$  to be used as a water mass ventilation tracer (e.g. Boyle and Keigwin, 1987; Curry and Oppo, 2005; Duplessy et al., 1988; Eide et al., 2017). The  $\delta^{13}\text{C}$  of benthic foraminifera shells, particularly of the species *Cibicides wuellerstorfi*, has been found to reliably represent the  $\delta^{13}\text{C}$  signature of DIC (Belanger et al., 1981; Duplessy et al., 1984; Zahn et al., 1986) and has therefore been used to better constrain the extent of different water masses. Mass balances of  $\delta^{13}\text{C}$  between the atmosphere, ocean and land have been previously used to constrain changes in terrestrial carbon between the Last Glacial Maximum (~20 ka BP) and Holocene (e.g. Peterson et al., 2014). However, on longer time scales, exchanges with the lithosphere including volcanic outgassing (Hasenklever et al., 2017; Huybers and Langmuir, 2009),  $\text{CaCO}_3$  burial in sediments and weathering, release of carbon from methane clathrates, and the net burial of organic carbon also influence the global mean  $\delta^{13}\text{C}$ . It has been estimated that the amount of carbon both entering and exiting the lithosphere due to weathering and burial of organic carbon fluxes could be from 0.274 to 0.344 Gt C yr<sup>-1</sup> (Schneider et al., 2013), though these vary through time (Hoogakker et al., 2006). Over timescales greater than 10 ka, the influence of weathering and burial of carbon might dominate the  $\delta^{13}\text{C}$  signal (Jeltsch-Thömmes et al., 2019; Jeltsch-Thömmes and Joos, 2020), so a mass balance cannot be accurately applied to evaluate terrestrial carbon changes between the LIG and Holocene.

Here, we present a new compilation of benthic  $\delta^{13}\text{C}$  from *Cibicides wuellerstorfi* spanning the 130–118 ka BP time period. We use this data to compare the  $\delta^{13}\text{C}$  signal of the LIG with that of the Holocene and to determine the difference in average ocean  $\delta^{13}\text{C}$  between the two time periods. We then investigate the AMOC during the LIG with our new benthic  $\delta^{13}\text{C}$  database. Finally, we qualitatively explore the role of the various processes affecting the  $\delta^{13}\text{C}$  difference between the LIG and the  
95 Holocene.

## 2 Database and methods

### 2.1 Database

We present a new compilation of benthic  $\delta^{13}\text{C}$  covering the periods 130–118 ka BP and 8–2 ka BP. From these two sets of data, we select data pertaining to the LIG and compare it to data from the Holocene. Our database only includes measurements on  
100 *Cibicides wuellerstorfi* as no significant fractionation between the calcite shells and the surrounding DIC has been measured in this species (Belanger et al., 1981; Duplessy et al., 1984; Zahn et al., 1986).

Our compilation is predominantly based on Lisiecki and Stern (2016) (53 cores), but includes 14 cores described in Oliver et al. (2010), as well as a few other records (CH69-K09 (Labeyrie et al., 2017), MD03-2664 (Galaasen et al., 2014a), MD95-2042 (Martrat et al., 2007a), ODP 1063 (Deaney et al., 2017), and U1304 (Hodell and Channell, 2016)). The full core lists are  
105 provided in Tables 1 and 2 for the LIG and the Holocene, respectively.

### 2.2 Age models

Due to the lack of absolute age markers, such as tephra layers, the LIG age models mostly rely on alignment strategies that tie each record to a well-dated reference record. The age model tie-points used in this study are taken from the original age model publications. The reference records (LS16, Lisiecki and Stern (2016)) consist of eight regional stacks (one for the  
110 intermediate and one for the deep ocean for each the North Atlantic, South Atlantic, Pacific and Indian Oceans) of benthic  $\delta^{18}\text{O}$  that were dated through alignment with other climatic archives such as ice-raftered debris records, synthetic ice core records and speleothems. The use of regional stacks, rather than a single global stack, improved stratigraphic alignment targets and provided more robust age models. The estimated age model uncertainty ( $2\sigma$ ) for this group of cores is 2 ka. Please refer to Lisiecki and Stern (2016) for further details. Oliver et al. (2010) defined their age tie points assuming that sea level minima  
115 and benthic  $\delta^{18}\text{O}$  maxima are synchronous. The benthic  $\delta^{18}\text{O}$  records were aligned with each other and then tied to the Dome Fuji chronology (based on  $\text{O}_2/\text{N}_2$ ) (Kawamura et al., 2007). Please refer to Shackleton et al. (2000) and Oliver et al. (2010) for an extensive method description. The age model uncertainty on this group of cores is estimated to range from 1 to 2.5 ka.

The published age models for the additional cores were determined using similar alignment techniques: SSTs were correlated to the NGRIP Greenland ice core for CH69-K09 and MD95-2042 (Govin et al., 2012). The age model for MD03-2664 was  
120 determined by correlating MD03-2664  $\delta^{18}\text{O}$  with previously dated MD95-2042  $\delta^{18}\text{O}$  (Galaasen et al., 2014b). ODP 1063 and U1304  $\delta^{18}\text{O}$  were originally aligned to the LR04 stack (Lisiecki and Raymo, 2005). In order to align all the records, adjustments

**Table 1.** List of cores for the last interglacial period (LIG). Provided is the core name ('Core'), latitude (Lat, °), longitude (Lon, °), depth (Dep, m), the region and the reference. Regions: NEA: northeast Atlantic, NWA: northwest Atlantic, SWA: southwest Atlantic, SEA: southeast Atlantic, SA: south Atlantic, NP: north Pacific, SP: south Pacific, I: Indian. Reference abbreviations: BW96: Bickert and Wefer (1996), CL82: Curry and Lohmann (1982), dA03: de Abreu et al. (2003), KJ8994: Keigwin and Jones (1989, 1994), KS02: Keigwin and Schlegel (2002), L99: Labeyrie et al. (1999), MB99: Mackensen and Bickert (1999), OH00: Oppo and Horowitz (2000), SH84: Shackleton and Hall (1984), SS0405: Skinner and Shackleton (2004, 2005), VH02: Venz and Hodell (2002), V99: Venz et al. (1999), ZM1011: Zarriess and Mackensen (2010, 2011).

Core	Lat	Lon	Dep (m)	Region	Reference	Core	Lat	Lon	Dep (m)	Region	Reference
ODP758	5.38	90.36	2,935	I	Chen et al. (1995)	SU90-39	52.5	-22	3,955	NEA	Cortijo (2003)
RC12-339	9.13	90.03	3,010	I	Members (2006)	ODP983	60.4	-23.64	1,984	NEA	McIntyre et al. (1999)
GEOB3004-I	14.61	52.92	1,803	I	Schmidell and Mackensen (2006)	SU90-03	40.05	-32	2,475	NEA	Chapman and Shackleton (1999)
MD01-2378	-13.08	121.79	1,783	I	Holbourn et al. (2005)	U1308	49.88	-24.24	3,883	NEA	Hodell et al. (2008)
Y69-71	0.1	-95.65	2,740	NP	Lyle et al. (2002)	ODP980	55.49	-14.7	2,168	NEA	McManus et al. (1999); Oppo et al. (1998)
ODP677	1.2	-83.73	3,450	NP	SH84, Shackleton et al. (1990)	ODP982	57.51	-15.85	1,134	NEA	Jansen et al. (1996); V99, VH02
ODP849	0.18	-110.52	3,839	NP	Shackleton et al. (1990)	EW9209-1JPC	5.91	-44.2	4,056	NWA	Curry and Oppo (1997)
V24-109	0.43	158.8	2,367	NP	Duplessy et al. (1984)	GEOB4403-2	6.13	-43.44	4,503	NWA	Bickert and Mackensen (2003)
Y69-106	2.98	-86.55	2,870	NP	Lyle et al. (2002); Pisias and Mix (1997)	ODP1063	33.68	-57.62	4,584	NWA	Deane et al. (2017)
ODP807A	3.61	156.63	2,804	NP	Zhang et al. (2007)	CH69-K9	41.75	-47.35	4,100	NWA	L99, Waelbroeck et al. (2001)
GIK17961-2	8.51	112.33	1,795	NP	Wang et al. (1999)	SU90-11	44.07	-40.02	3,645	NWA	Julien et al. (2006); Labeyrie et al. (1995)
MD97-2151	8.73	109.87	1,598	NP	Lee et al. (1999); Wei et al. (2006)	U1304	53.06	-33.53	3,065	NWA	Hodell and Channell (2016)
ODP1143	9.36	113.29	2,772	NP	Cheng et al. (2004)	V27-20	54.0	-46.2	3,510	NWA	Ruddiman and Members (1982)
V28-304	28.53	134.13	2,942	NP	Duplessy et al. (1984)	MD03_2664	57.44	-48.61	3,442	NWA	Galbraith et al. (2014a)
V32-128	36.47	177.17	3,623	NP	Duplessy et al. (1984)	ODP925	4.2	-43.49	3,040	NWA	Bickert et al. (1997)
PS2495	-41.28	-14.49	3,134	SA	Mackensen et al. (2001)	ODP926	3.72	-42.91	3,598	NWA	Curry et al. (1995)
ODP1089	-40.94	9.89	4,621	SA	Hodell et al. (2001)	ODP928	5.46	-43.75	4,012	NWA	Bickert et al. (1997)
PS2082	-43.22	11.74	4,610	SA	McCorkle and Holder (2001)	V28-127	11.65	-80.13	3,237	NWA	Oppo and Fairbanks (1987)
MD06-3018	-23	166.15	2,470	SP	Russon et al. (2009)	KNR140-37JPC	31.41	-75.26	3,000	NWA	Curry and Oppo (2005), KS02
RC13-110	-0.1	-95.65	3,231	SP	Mix et al. (1991)	GEOB3801-6	-29.51	-8.31	4,546	SEA	Bickert and Mackensen (2003)
ODP846	-3.1	-90.82	3,296	SP	Shackleton et al. (1995)	GEOB1214	-24.69	7.24	3,210	SEA	BW96
V19-27	-0.47	-82.07	1,373	SP	Mix et al. (1991)	GEOB1211	-24.48	7.53	4,084	SEA	BW96
GEOB1101	1.66	-10.98	4,588	NEA	BW96	GEOB170	-23.43	11.7	2,987	SEA	Schmidell and Mackensen (1997)
GIK13519-1	5.67	-19.95	2,862	NEA	Zahn et al. (1986)	GEOB1034	-21.74	5.42	3,772	SEA	BW96
GIK16402	14.42	-20.54	4,202	NEA	Sarnthein et al. (1994)	GEOB1035	-21.59	5.03	4,453	SEA	BW96
GIK12392-1	25.17	-16.85	2,573	NEA	Shackleton (1977); Zahn et al. (1986)	GEOB1028-5	-20.1	9.19	2,209	SEA	Bickert and Mackensen (2003)
GIK16004	29.98	-10.65	1,512	NEA	Sarnthein et al. (1994)	V22-174	-10.07	-12.82	2,630	SEA	Shackleton (1977)
GEOB4216	30.63	-12.4	2,324	NEA	Freudenthal et al. (2002)	GEOB1112	-5.78	-10.75	3,125	SEA	BW96, MB99
GIK15669	34.89	-7.82	2,022	NEA	Sarnthein et al. (1994)	GEOB1115	-3.56	-12.56	2,945	SEA	BW96, MB99
GIK15612-2	44.36	-26.54	3,050	NEA	Sarnthein et al. (1994)	GEOB1041	-3.48	-7.6	4,033	SEA	BW96, MB99
NO79-28	45.63	-22.75	3,625	NEA	Duplessy (1996)	GIK16867	-2.2	5.1	3,891	SEA	Sarnthein et al. (1994)
GIK23416-4	51.57	-20.0	3,616	NEA	Sarnthein et al. (1994)	GEOB1105	-1.67	-12.43	3,225	SEA	BW96, MB99
NEAP18K	52.77	-30.35	3,275	NEA	Chapman and Shackleton (1999)	GIK16772-1	-1.34	-11.97	3,911	SEA	Sarnthein (2003)
GIK23415-9	53.18	-19.15	2,472	NEA	CL82, Sarnthein et al. (1994)	V29-135	-19.7	8.88	2,675	SEA	Sarnthein et al. (1994)
GIK23414-9	53.54	-20.29	2,196	NEA	Sarnthein et al. (1994)	RC13-228	-22.33	11.2	3,204	SEA	Bickert and Mackensen (2003)
CH73-139	54.63	-16.35	2,209	NEA	Curry et al. (1988); Sarnthein et al. (1994)	ODP1087	-31.46	15.31	1,372	SEA	Lynch-Stieglitz et al. (2006)
GIK17049-6	55.26	-26.73	3,331	NEA	Sarnthein et al. (1994)	MD96-2080	-36.27	19.48	2,488	SEA	Rau et al. (2002)
V28-56	68.03	-6.12	2,941	NEA	Ruddiman and Members (1982)	GEOB2109-1	-27.91	-45.88	2,504	SWA	Vidal et al. (1999)
ODP984	61	-24	1,650	NEA	Raymo et al. (2004)	V22-38	-9.55	-34.25	3,797	SWA	Ruddiman and Members (1982)
V29-202	61	-21	2,658	NEA	Oppo and Lehman (1995)	GEOB1117	-3.82	-14.9	3,984	SWA	BW96, MB99
ODP664	0.11	-23.23	3,806	NEA	Raymo et al. (1997)	GEOB1118	-3.56	-16.43	4,675	SWA	BW96, MB99

to the age models of cores from Oliver et al. (2010) and the five additional cores (CH69-K09, MD95-2042, MD03-2664, ODP 1063 and U1304) were made by aligning the  $\delta^{18}\text{O}$  minima during the LIG to the corresponding  $\delta^{18}\text{O}$  minima of the nearest LS16 stack. The  $\delta^{18}\text{O}$  data before and after the alignment is given in Fig. S1.

The Holocene age models are based on planktonic foraminifera radiocarbon dates (Stern and Lisiecki, 2014; Waelbroeck et al., 2001), which have been converted into calendar ages using IntCal13 and using reservoir ages based on modern observations (Key et al., 2004), which are assumed to have remained fairly stable across the Holocene. The age uncertainty associated with these Holocene radiocarbon-based age models is generally less than 0.5 ka. However, it is important to note that Holocene age models from Oliver et al. (2010) were derived using the same method as their LIG age models, leading to larger age uncertainties of about 1–2.5 ka for this set of Holocene records (4 cores). The tie points were used to derive a full age-depth model assuming a constant sedimentation rate between tie-points (i.e. linear interpolation).

**Table 2.** List of cores for the Holocene. Provided is the core name ('Core'), latitude (Lat, °), longitude (Lon, °), depth (Dep, m) the region and the reference. Regions: NEA: northeast Atlantic, NWA: northwest Atlantic, SWA: southwest Atlantic, SEA: southeast Atlantic, SA: south Atlantic, NP: north Pacific, SP: south Pacific, I: Indian. Reference abbreviations: BW96: Bickert and Wefer (1996), CL82: Curry and Lohmann (1982), dA03: de Abreu et al. (2003), KJ8994Keigwin and Jones (1989, 1994), KS02: Keigwin and Schlegel (2002), L99: Labeyrie et al. (1999), MB99: Mackensen and Bickert (1999), OH00: Oppo and Horowitz (2000), SH84: Shackleton and Hall (1984), SS0405: Skinner and Shackleton (2004, 2005), VH02: Venz and Hodell (2002), V99: Venz et al. (1999), ZM1011: Zarriess and Mackensen (2010, 2011).

Core	Lat	Lon	Dep (m)	Region	Reference	Core	Lat	Lon	Dep (m)	Region	Reference
ODP758	5.38	90.36	2,935	I	Chen et al. (1995)	GIK23419	54.96	-19.76	1,487	NEA	Sarnthein et al. (1994)
GEOB3004-1	14.61	52.92	1,803	I	Schmid and Mackensen (2006)	GIK17049-6	55.26	-26.73	3,331	NEA	Sarnthein et al. (1994)
M5-3A-422	24.39	58.04	2,732	I	Sirocko et al. (2000)	DSDP552	56.04	-23.22	2,311	NEA	SH84
MD01-2378	-13.08	121.79	1,783	I	Holbourn et al. (2005)	GIK17051	56.16	-31.99	2,295	NEA	Sarnthein et al. (1994)
MD79-254	-17.53	38.4	1,934	I	Curry et al. (1988)	GIK23519	64.8	-29.6	1,893	NEA	Millo et al. (2006)
RC11-120	-43.52	79.87	3,193	I	CL82	ODP984	61	-24	1,650	NEA	Raymo et al. (2004)
MD88-770	-46.02	96.46	3,290	I	Labeyrie et al. (1996); Sowers et al. (1993)	V29-202	61	-21	2,658	NEA	Oppo and Lehman (1995)
V35-5	7.2	112.08	1,953	NP	Wang et al. (1999)	MD95-2042	37.8	-10.17	3,146	NEA	Martrat et al. (2007a)
V24-109	0.43	158.8	2,367	NP	Duplessy et al. (1984)	SU90-39	52.5	-22	3,955	NEA	Corrijo (2003)
Y69-106	2.98	-86.55	2,870	NP	Lyle et al. (2002); Pisias and Mix (1997)	ODP983	60.4	-23.64	1,984	NEA	McIntyre et al. (1999)
ODP807A	3.61	156.63	2,804	NP	Zhang et al. (2007)	V22-197	14.17	-18.58	3,167	NEA	Sarnthein et al. (1994)
GIK17964-2	6.16	112.21	1,556	NP	Wang et al. (1999)	ODP659	18.08	-21.03	3,082	NEA	Sarnthein et al. (1994)
GIK17961-2	8.51	112.33	1,795	NP	Wang et al. (1999)	V30-49	18.43	-21.08	3,093	NEA	Mix and Fairbanks (1985)
MD97-2151	8.73	109.87	1,598	NP	Lee et al. (1999); Wei et al. (2006)	MD03-2698	38.24	-10.39	4,602	NEA	Lebreiro et al. (2009)
GIK17940-2	20.12	117.38	1,727	NP	Wang et al. (1999)	SU90-03	40.05	-32	2,475	NEA	Chapman and Shackleton (1999)
V28-304	28.53	134.13	2,942	NP	Duplessy et al. (1984)	V23-81	54.25	-16.83	2,393	NEA	Sarnthein et al. (1994)
EW9504-05	32.48	-118.13	1,818	NP	Stott et al. (2000)	NA87-22	55.48	-14.68	2,161	NEA	Sarnthein et al. (1994)
MD02-2489	54.39	-148.92	3,640	NP	Gebhardt et al. (2008)	ODP980	55.49	-14.7	2,168	NEA	Oppo et al. (1998); McManus et al. (1999)
ODP1090	-42.91	8.9	3,702	SA	Hodell et al. (2000, 2003)	ODP982	57.51	-15.85	1,134	NEA	Jansen et al. (1996), V99, VH02
ODP1089	-40.94	9.89	4,621	SA	Hodell et al. (2001)	V28-14	64.78	-29.57	1,855	NEA	Duplessy et al. (1984)
PS2082	43.22	11.74	4,610	SA	McCorkle and Holder (2001)	KNR110-50	4.87	-43.21	3,995	NWA	Curry et al. (1988)
MD07-3076	-44.07	-14.21	3,770	SA	Waelbroeck et al. (2011)	KNR110-55	4.95	-42.89	4,556	NWA	Curry et al. (1988)
MD06-3018	-23	166.15	2,470	SP	Russon et al. (2009)	EW9209-JPC	5.91	-44.2	4,056	NWA	Curry and Oppo (1997)
RC13-110	-0.1	-95.65	3,231	SP	Mix et al. (1991)	GEOB4403-2	6.13	-43.44	4,503	NWA	Bickert and Mackensen (2003)
ODP846	-3.1	-90.82	3,296	SP	Shackleton et al. (1995)	KNR31-GPC5	33.69	-57.63	4,583	NWA	KJ8994, Keigwin et al. (1991)
V19-27	-0.47	-82.07	1,373	SP	Mix et al. (1991)	CH69-K9	41.75	-47.35	4,100	NWA	L99, Waelbroeck et al. (2001)
H214	-36.92	177.43	2,045	SP	Samson et al. (2005)	U1304	53.06	-33.53	3,065	NWA	Hodell and Channell (2016)
RS147-07	-45.15	146.28	3,300	SP	Sikes et al. (2009)	ODP925	4.2	-43.49	3,040	NWA	Bickert et al. (1997)
MD97-2120	-45.53	174.93	1,210	SP	Pahnke and Zahn (2005)	V25-59	1.37	-33.48	3,824	NWA	Mix and Fairbanks (1985)
GEOB1101	1.66	-10.98	4,588	NEA	BW96	ODP226	3.72	-42.91	3,598	NWA	Curry et al. (1995)
EN066-29	2.46	-19.76	5,105	NEA	Sarnthein et al. (1994)	KNR110-75	4.34	-43.41	3,063	NWA	Curry et al. (1988)
EN066-32	2.47	-19.73	4,998	NEA	Sarnthein et al. (1994)	KNR110-82	4.34	-43.49	2,816	NWA	Curry et al. (1988)
EN066-26	3.09	-20.02	4,745	NEA	Sarnthein et al. (1994)	KNR110-71	4.36	-43.7	3,164	NWA	Curry et al. (1988)
EN066-21	4.23	-20.63	3,792	NEA	Sarnthein et al. (1994)	KNR110-66	4.56	-43.38	3,547	NWA	CL82, Curry et al. (1988)
EN066-36	4.31	-20.21	4,095	NEA	Boyle (1992)	KNR110-91	4.76	-43.31	3,810	NWA	Curry et al. (1988)
EN066-38	4.92	-20.5	2,937	NEA	Sarnthein et al. (1994)	KNR110-58	4.79	-43.04	4,341	NWA	Curry et al. (1988)
EN066-44	5.26	-21.71	3,423	NEA	Sarnthein et al. (1994)	ODP927	5.46	-44.48	3,326	NWA	Bickert et al. (1997)
EN066-16	5.45	-21.14	3,160	NEA	Boyle (1992)	ODP928	5.46	-43.75	4,012	NWA	Bickert et al. (1997)
GIK13519-1	5.67	-19.85	2,862	NEA	Zahn et al. (1986)	ODP929	5.98	-43.74	4,369	NWA	Bickert et al. (1997)
EN066-10	6.64	-21.9	3,527	NEA	Sarnthein et al. (1994)	V28-127	11.65	-80.13	3,237	NWA	Oppo and Fairbanks (1987)
GEOB9526	12.44	-18.06	3,223	NEA	ZM1011, Zarriess et al. (2011)	M35003-4	12.09	-61.24	1,299	NWA	Hüls (1999); Zahn and Stüber (2002)
GIK16402	14.42	-20.54	4,202	NEA	Sarnthein et al. (1994)	KNR140-37JPC	31.41	-75.26	3,000	NWA	Curry and Oppo (2005), KS02
GEOB9508-5	14.5	-17.95	2,384	NEA	Multizta et al. (2008)	V26-176	36.05	-72.38	3,942	NWA	Curry et al. (1988)
GIK12347-2	15.83	-17.86	2,576	NEA	Sarnthein et al. (1994)	GEOB1214	-24.69	7.24	3,210	SEA	BW96
GE0B7920-2	20.75	-18.58	2,278	NEA	Collins et al. (2011); Tjallingii et al. (2008)	GEOB1211	-24.48	7.53	4,084	SEA	BW96
GIK12328-5	21.15	-18.57	2,778	NEA	Sarnthein et al. (1994)	GEOB1710	-23.43	11.7	2,987	SEA	Schmid and Mackensen (1997)
GIK16030	21.24	-18.06	1,516	NEA	Sarnthein et al. (1994)	GEOB1032	-22.92	6.04	2,505	SEA	BW96, Bickert et al. (2003)
GIK12379-3	23.14	-17.75	2,136	NEA	Sarnthein et al. (1994)	GEOB1034	-21.74	5.42	3,772	SEA	BW96
GIK12392-1	25.17	-16.85	2,573	NEA	Shackleton (1977); Zahn et al. (1986)	GEOB1035	-21.59	5.03	4,453	SEA	BW96
GE0B4240	28.89	-13.23	1,358	NEA	Freudenthal et al. (2002)	GEOB1028-5	-20.1	9.19	2,209	SEA	Bickert and Mackensen (2003)
GIK16004	29.98	-10.65	1,512	NEA	Sarnthein et al. (1994)	GEOB1112	-5.78	-10.75	3,125	SEA	BW96, MB99
GE0B4216	30.63	-12.4	2,324	NEA	Freudenthal et al. (2002)	BT4	-4.0	10.0	1,000	SEA	Sarnthein et al. (1994)
GIK15672	34.86	-8.13	2,460	NEA	CL82, Sarnthein et al. (1994)	GEOB1115	-3.56	-12.56	2,945	SEA	BW96, MB99
GIK15669	34.89	-7.82	2,022	NEA	Sarnthein et al. (1994)	GEOB1041	-3.48	-7.6	4,033	SEA	BW96, MB99
GIK1944-2	35.65	-8.06	1,765	NEA	Sarnthein et al. (1994)	GIK16867	-2.2	5.1	3,891	SEA	Sarnthein et al. (1994)
KF13	37.58	-31.84	2,690	NEA	Curry et al. (1988)	GEOB1105	-1.67	-12.43	3,225	SEA	BW96, MB99
MD99-2334	37.8	-10.17	3,146	NEA	Skinner et al. (2003), SS0405	V29-135	-19.7	8.88	2,675	SEA	Sarnthein et al. (1994)
MD95-2040	40.58	-9.86	2,465	NEA	dA03, Schönfeld et al. (2003)	RC13-229	-25.5	11.3	4,194	SEA	Sarnthein et al. (1994)
CHN82-24	41.72	-32.85	3,427	NEA	Boyle and Keigwin (1985)	RC13-228	-22.33	11.2	3,204	SEA	Bickert and Mackensen (2003)
GIK15612-2	44.36	-26.54	3,050	NEA	Sarnthein et al. (1994)	ODP1087	-31.46	15.31	1,372	SEA	Lynch-Stieglitz et al. (2006)
NO79-28	45.63	-22.75	3,625	NEA	Duplessy (1996)	MD96-2080	-36.27	19.48	2,488	SEA	Rau et al. (2002)
GIK17055-1	48.22	-27.06	2,558	NEA	Sarnthein et al. (1994)	GEOB2109-1	-27.91	-45.88	2,504	SWA	Vidal et al. (1999)
U1308	49.88	-24.24	3,883	NEA	Hodell et al. (2008)	KNR159-36	-27.51	-46.47	1,268	SWA	Cane et al. (2003), OH00
GIK23417-1	50.67	-19.43	3,850	NEA	Sarnthein et al. (1994)	GEOB1117	-3.82	-14.9	3,984	SWA	BW96, MB99
GIK23416-4	51.57	-20.0	3,616	NEA	Sarnthein et al. (1994)	GEOB1118	-3.56	-16.43	4,675	SWA	BW96, MB99
GIK23418-8	52.55	-20.33	2,841	NEA	Sarnthein et al. (1994)	RC16-84	-26.7	-43.33	2,438	SWA	OH00
GIK23415-9	53.18	-19.15	2,472	NEA	CL82, Sarnthein et al. (1994)	RC16-119	-27.7	-46.52	1,567	SWA	OH00
GIK23414-9	53.54	-20.29	2,196	NEA	Sarnthein et al. (1994)	V24-253	-26.95	44.67	2,069	SWA	OH00

## 2.3 Spatial coverage

The spatial distribution of the database for the Holocene and the LIG is shown in Fig. 2 and the depth distribution in each ocean basin is shown in Fig. 3. There is more data in the Atlantic Ocean (65 LIG, 118 Holocene) than in the Pacific (15 LIG, 19 Holocene) and Indian (3 LIG, 7 Holocene) Oceans. We used this database to determine 1) if there is a significant difference in the average ocean  $\delta^{13}\text{C}$  signal at the LIG compared to the Holocene, and 2) if ocean circulation patterns were comparable. Due to the sparsity of data in the Indian and Pacific Oceans, our investigation is primarily focused on the Atlantic. Additionally, the temporal uncertainties ( $\sim 2$  ka) do not permit an investigation of centennial-scale events, and therefore we restrict our analysis to mean LIG and Holocene conditions.

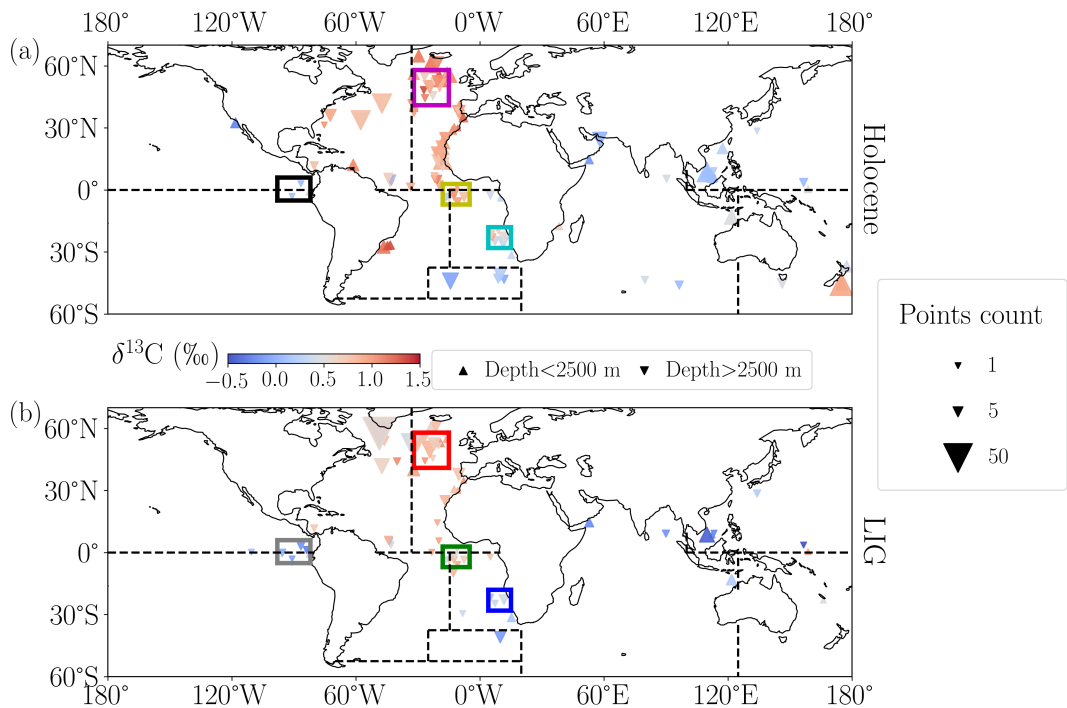


**Figure 2.** Global distribution of benthic foraminifera  $\delta^{13}\text{C}$  covering the periods studied here: the Holocene (7–2 ka BP) (a) and LIG (125–120 ka BP) (b). Symbol size indicates the number of values per core, colour indicates average  $\delta^{13}\text{C}$ , and the triangle direction indicates the proxy depth (upward-pointing triangle: between 1,000 and 2,500 m depth, downward-pointing triangle: deeper than 2,500 m). Four specific regions used in Sect. 3.1 are outlined: eastern equatorial Pacific (black, grey), equatorial Atlantic (yellow, green), southeast Atlantic (cyan, blue), and northeast Atlantic (magenta, red). Regional boundaries used to calculate the global volume-weighted mean  $\delta^{13}\text{C}$  (Sect. 3.2) are indicated by dotted black lines as defined in Peterson et al. (2014).

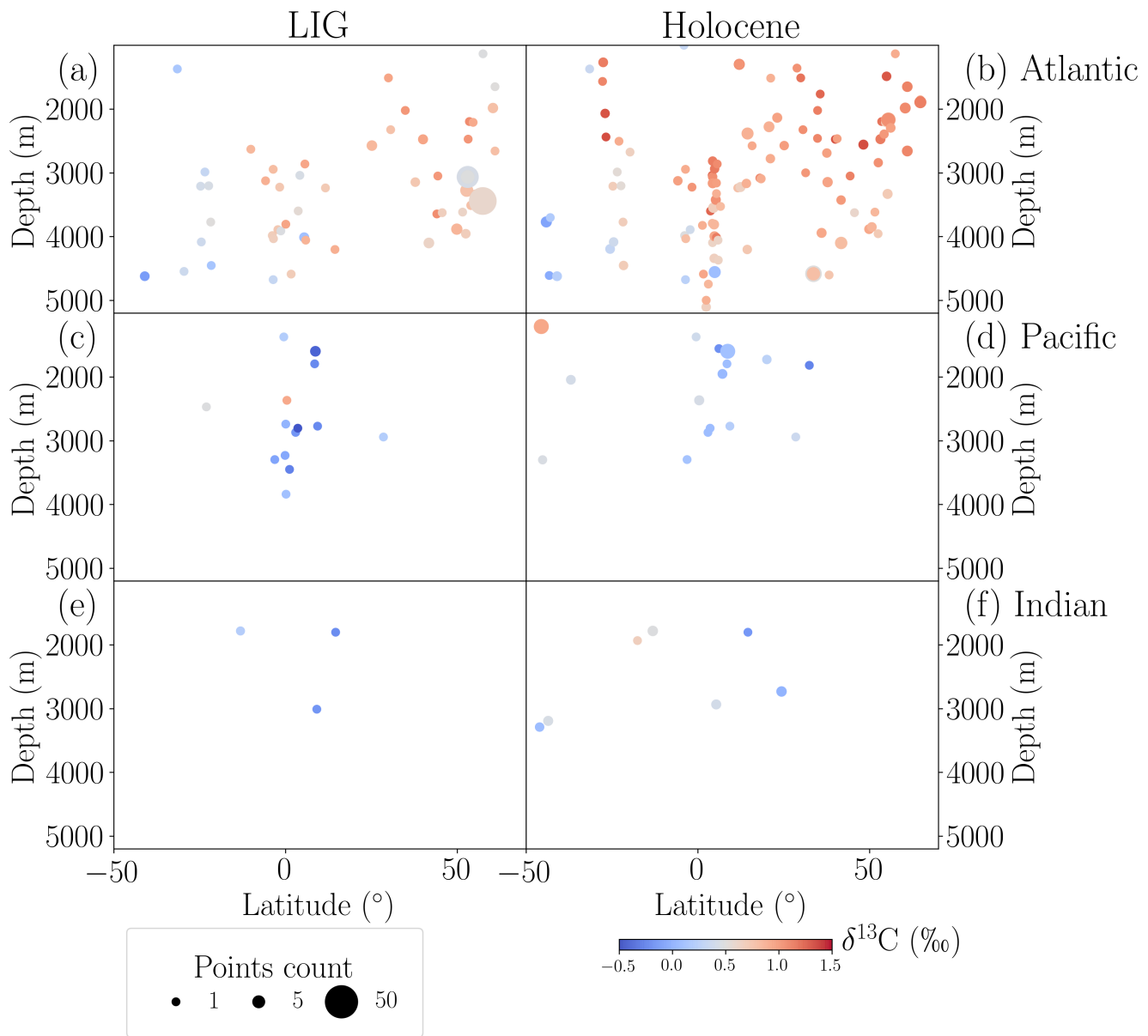


**Figure 3.** Zonal distribution of benthic foraminifera  $\delta^{13}\text{C}$  (‰) during the LIG (125–120 ka BP; a, c, e) and the Holocene (7–2 ka BP; b, d, f) in the Atlantic Ocean (a, b), Pacific Ocean (c, d) and Indian Ocean (e, f). Symbol size indicates the number of measurements per core and colour indicates average  $\delta^{13}\text{C}$ .

The  $\delta^{13}\text{C}$  signal varies significantly regionally and with depth. The highest average  $\delta^{13}\text{C}$  values are associated with NADW and are generally found at depths between  $\sim 1,500$  and  $3,000$  m in the North Atlantic, with organic matter remineralisation and mixing with southern source waters leading to a  $\delta^{13}\text{C}$  decrease along the NADW path. The lowest  $\delta^{13}\text{C}$  values are in the deep south Atlantic ( $>4,000$  m) because the Antarctic Bottom Water (AABW) end member is much lower than its NADW counterpart. Since the Indian and Pacific Oceans are mostly ventilated from southern-sourced water masses,  $\delta^{13}\text{C}$  generally decreases northward in these two basins.

Since the number of cores is not consistent across the two time periods, and given the high regional variability observed in  $\delta^{13}\text{C}$ , it is not possible to simply average all available data to determine the global mean  $\delta^{13}\text{C}$ . Furthermore, the spatial heterogeneity of the data density adds to the complexity of the problem. To address these points, we first analyse differences between the LIG and Holocene records for pre-defined small regions with high data density. We then calculate regional volume-weighted  $\delta^{13}\text{C}$  means for larger regions from which we estimate the global LIG-Holocene anomaly.

### 3.1 Regional reconstruction of $\delta^{13}\text{C}$

We define regions with high densities of cores to reconstruct regional mean  $\delta^{13}\text{C}$  (Fig. 2). These regions need to be small enough to assume reasonably small spatial variability in the  $\delta^{13}\text{C}$  signal and yet still have enough data to establish a reliable statistical difference between the two time periods.

Based on these requirements, four regions are selected: the northeast Atlantic, the equatorial Atlantic, a region off the Namibian Coast (southeast Atlantic), and a region around the Galapagos Islands (eastern equatorial Pacific). The boundaries of each region are defined in Table 3.

We then define the time periods within the LIG and the Holocene to perform our analyses. For the Holocene, as most of the available data is dated prior to 2 ka BP, we define the end of our Holocene time period as 2 ka BP. To capture as much of the Holocene data as possible, we include data back to 7 ka BP, ensuring that we do not include instability associated with the 8.2 kiloyear event (Alley and Ágústsdóttir, 2005; Thomas et al., 2007). This provides a time span of 5 ka of data that we will consider for our analysis of the Holocene.

For the LIG, we seek to avoid data associated with the end of the penultimate deglaciation, which is characterised by a benthic  $\delta^{13}\text{C}$  increase in the Atlantic until  $\sim 128$  ka BP (Govin et al. (2015); Meniel et al. (2019); Oliver et al. (2010), Fig. 4). In addition, a millennial-scale event has been identified in the North Atlantic between  $\sim 127$  and  $126$  ka BP (Galaasen et al., 2014b; Tzedakis et al., 2018). Considering the typical dating uncertainties associated with the LIG data (2 ka), we thus decide to start our LIG time period at 125 ka BP. To ensure that the two time periods are of same length (5 ka BP), we define the LIG period for our analysis to be 125–120 ka BP. We note that our definition should also avoid data associated with the glacial inception (Govin et al., 2015; of PAGES, 2016). We verify that the LIG time period has sufficient data across the selected four regions, noting that the highest density of data falls within the 125–120 ka BP time period—particularly in the equatorial Atlantic and southeast Atlantic (Fig. 4b, c).

**Table 3.** Regional summary of  $\delta^{13}\text{C}$  below 2,500 m depth for the LIG (125–120 ka BP) and Holocene (7–2 ka BP) using a single value per core for each time slice. Shown are the non-volume-weighted means ( $\delta^{13}\text{C}$ , ‰), standard deviations ( $\sigma$ , ‰), and counts (N) for both time periods, along with the time period regional anomalies ( $\Delta\delta^{13}\text{C}$ , ‰), propagated standard deviations for the anomaly ( $\sigma$ , ‰), and p-values from two-sample t-tests between the two time periods.

Region	Latitude	Longitude	Holocene			LIG			LIG-Holocene		
			$\delta^{13}\text{C}$ (‰)	$\sigma$ (‰)	N	$\delta^{13}\text{C}$ (‰)	$\sigma$ (‰)	N	$\Delta\delta^{13}\text{C}$ (‰)	$\sigma$ (‰)	P value
Northeast Atlantic	41N-58N	32E-15E	0.89	0.21	34	0.76	0.11	23	-0.13	0.12	0.0096
Equatorial Atlantic	7S-3N	18E-5E	0.79	0.32	22	0.62	0.23	14	-0.17	0.20	0.1110
Southeast Atlantic	28S-18S	4W-15W	0.55	0.22	27	0.40	0.11	12	-0.15	0.12	0.0361
Equatorial Pacific	5S-6N	98E-82E	0.09	0.05	4	-0.11	0.10	8	-0.20	0.06	0.0056

We round the data to the nearest 1 ka, find an average per 1 ka, and refer to this as a time slice. We consider the LIG-Holocene anomaly across these two time periods for the four regions selected, and consider qualitatively the influence of changes in the  
175 average depth in which the proxies were recorded, as indicated by the direction of the black triangles in Fig. 4.

The average  $\delta^{13}\text{C}$  anomaly between the LIG and Holocene periods for cores deeper than 2,500 m is consistent across the different regions despite their geographic separation, suggesting a significantly lower  $\delta^{13}\text{C}$  during the LIG than the Holocene, with differences ranging from -0.13 ‰ in the northeast Atlantic to -0.20 ‰ in the equatorial Pacific (Table 3). The statistical significance between the two time periods is established using a two-tailed t-test on data of one mean value per core and  
180 spans the entire time slices (125–120 ka BP and 7–2 ka BP). The t-test shows that there is a statistically significant difference everywhere except in the equatorial Atlantic, with confidence intervals varying from 0.13 in the equatorial Atlantic to 0.04 in the northeast Atlantic. When using a single tail t-test instead, the difference becomes significant in the equatorial Atlantic, giving a new p-value of 0.02. Fig. 4 suggests that the difficulty in determining significance in this region for cores deeper than 2,500 m might be due to a singular outlier measurement in the equatorial Atlantic; a value of -0.23 ‰ from GeoB1118 at ∼3.5  
185 ka BP. If this value is excluded, then an anomaly of -0.22 with a p-value less than 0.005 is observed.

We also compare the distribution of  $\delta^{13}\text{C}$  for cores deeper than 2,500 m for three overlapping periods within the LIG (early LIG: 128–123 ka BP; LIG: 125–120 ka BP; late LIG: 123–118 ka BP). The results for the four regions are shown in Fig. 5. The statistical characteristics do not show much variation between the LIG and late LIG  $\delta^{13}\text{C}$  distributions. In the equatorial Pacific, the difference between the early LIG and the Holocene is smaller than between the LIG and Holocene, but this is countered  
190 with a larger difference in the equatorial Atlantic between early LIG and Holocene. The spread in the data is generally larger during the Holocene than during the other time periods which might be due to the greater number of measurements during the Holocene. The spread of data during the early LIG is slightly larger than during the LIG and late LIG in the equatorial and southeast Atlantic. The equatorial Atlantic is the only region which displays significantly more points with lower  $\delta^{13}\text{C}$  during the early LIG. Overall, these distributions do not suggest that the LIG-Holocene anomalies that we have determined would be  
195 significantly impacted by slight variations in the selected time window. We perform an analysis of variance (ANOVA) on each region and post hoc tests on the data. We find that the Holocene data is significantly different from the three LIG periods in the northeast Atlantic, the southeast Atlantic and the equatorial Pacific, while the three periods within the LIG are not significantly different from each other for any of the regions.

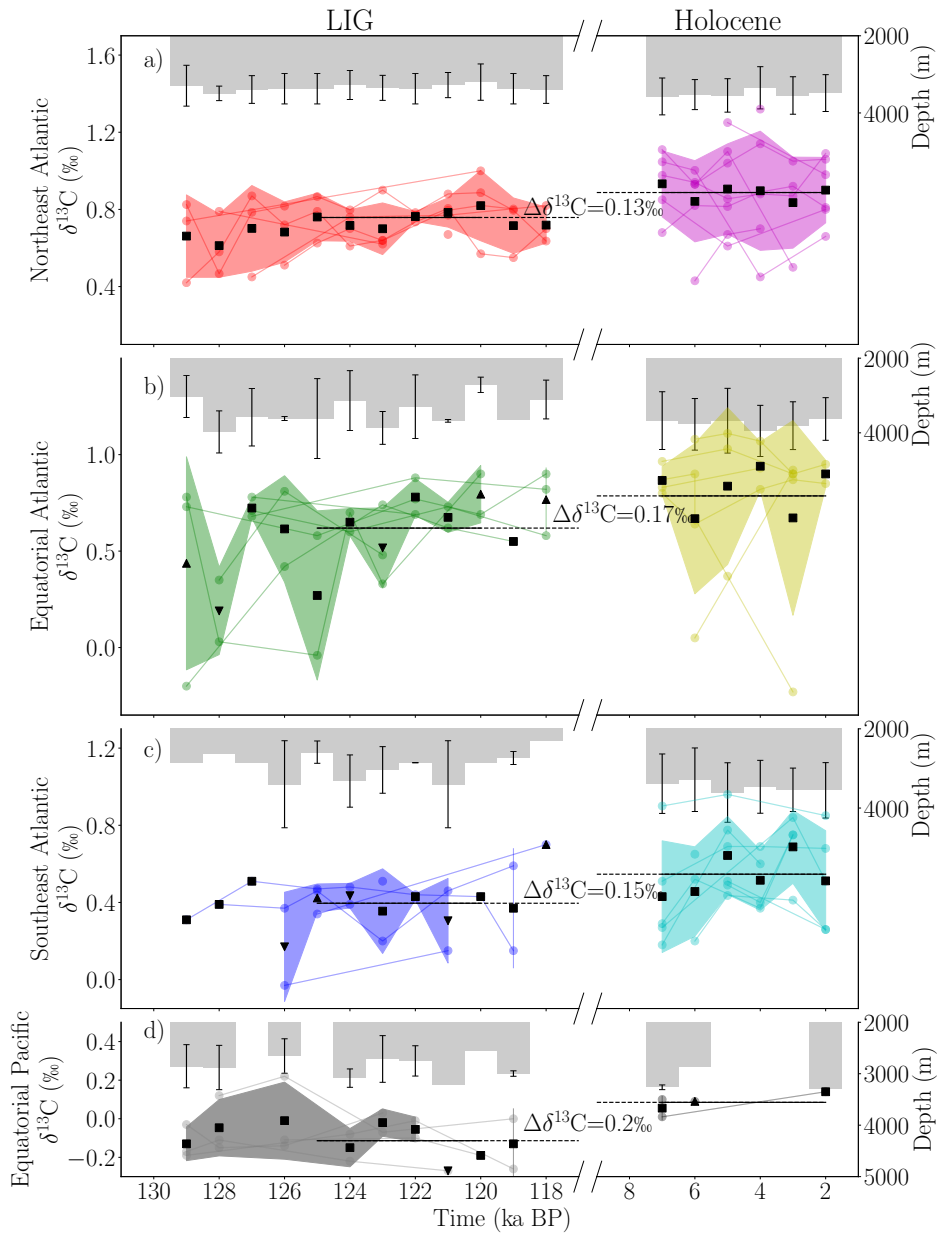


**Figure 4.** Benthic foraminifera  $\delta^{13}\text{C}$  (left y-axis, ‰) during the LIG (left) and Holocene (right) for four defined regions; northeast Atlantic (a), equatorial Atlantic (b), southeast Atlantic (c), and eastern equatorial Pacific (d). Data is presented in discrete time slices spanning 1 ka. Only cores deeper than 2,500 m are shown. Circular, coloured points connected by lines show each average  $\delta^{13}\text{C}$  value per core per time slice. Black symbols represent  $\delta^{13}\text{C}$  averages per slice. Each slice has a corresponding averaged depth (right y-axis, m), with 1 standard deviation on either side shown in the bars. Slices with an average depth within  $\pm 300$  m of the mean core depth of all slices are represented with a square point. Slices with an average depth shallower than 300 m less than the mean are shown with an upward triangle, and deeper than 300 m more than the mean are shown with a downward triangle. Shading shows 1 standard deviation on either side of the mean for slices where more than 1 point exists.

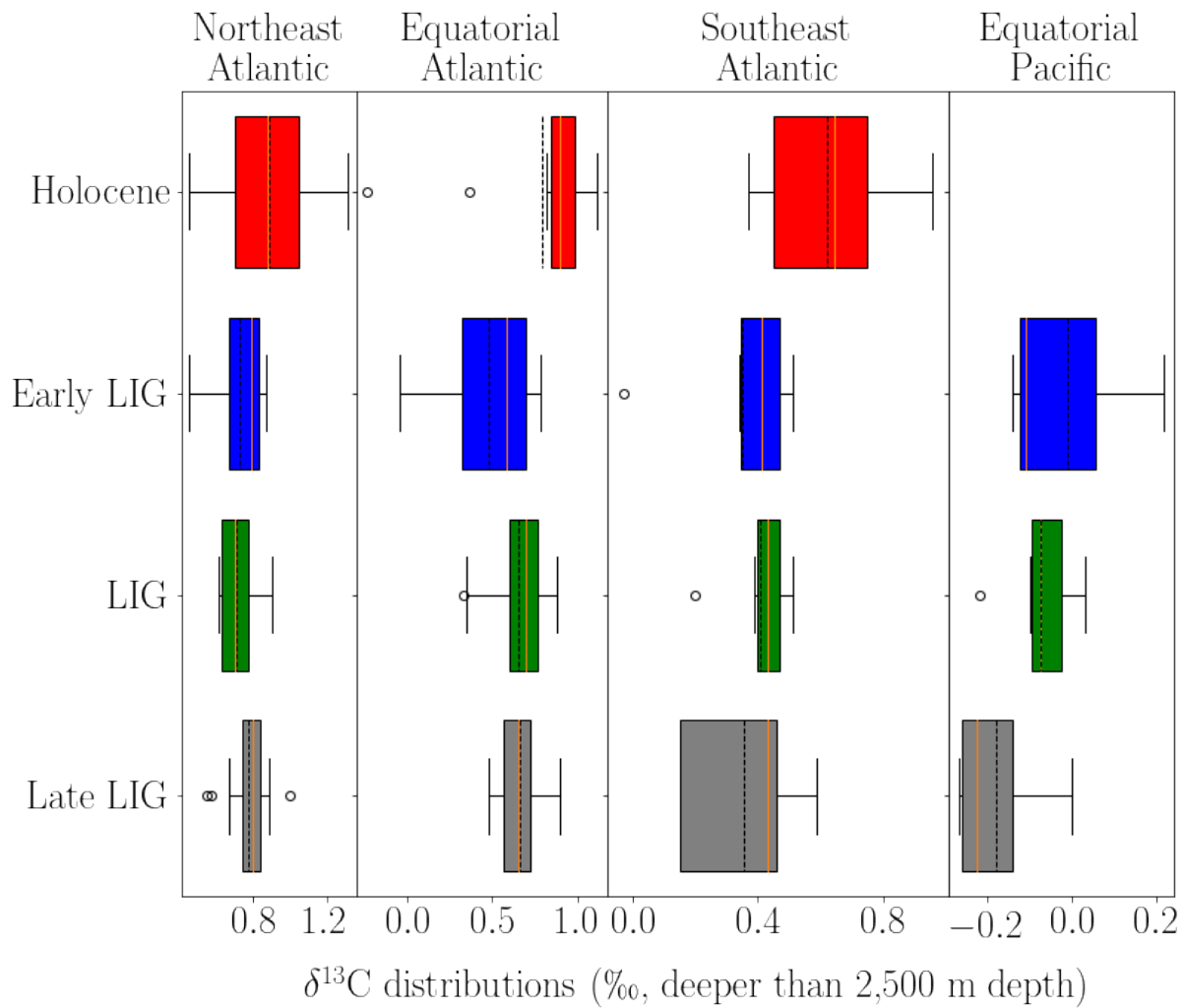


**Figure 5.** Distributions of  $\delta^{13}\text{C}$  for all core measurements deeper than 2,500 m during the Holocene (7–2 ka BP, red), the early LIG (128–123 ka BP), the LIG (125–120 ka BP), and the late LIG (123–118 ka BP) across four regions (equatorial Pacific, equatorial Atlantic, southeast Atlantic, northeast Atlantic). Lower end of the box indicates quartile 1 (Q1) and the upper end indicates quartile 3 (Q3). Orange vertical lines show the median and dotted vertical lines show the mean. The whiskers indicate the lower and upper fences of the data calculated as  $Q1-1.5*(Q3-Q1)$  and  $Q3+1.5*(Q3-Q1)$ , respectively, and the clear circles are outliers.

**Table 4.** Regional breakdown of  $\delta^{13}\text{C}$  data for all depths during the Holocene (7–2 ka BP) and LIG (125–120 ka BP) averaged across the 1 ka time slices. For each region: the average number of data points (labelled as ‘Points’) and cores per time slice (labelled as ‘Cores’), the average standard deviation of  $\delta^{13}\text{C}$  per time slices (‰), the mean depth (m) across time slices, and the standard deviation of depth (m) between time slices ( $\sigma_{depth}$ ). NEA: northeast Atlantic, NWA: northwest Atlantic, SA: south Atlantic, SEA: southeast Atlantic, SWA: southwest Atlantic, I: Indian, NP: north Pacific, SP: south Pacific.

Area	Holocene					LIG						
	$\delta^{13}\text{C}$ (‰)	Points	Cores	$\sigma_{\delta^{13}\text{C}}$ (‰)	Mean depth (m)	$\sigma_{depth}$ (m)	$\delta^{13}\text{C}$ (‰)	Points	Cores	$\sigma_{\delta^{13}\text{C}}$ (‰)	Mean depth (m)	$\sigma_{depth}$ (m)
NEA	0.94	73	47	0.19	2853	944	0.76	32	22	0.21	2746	789
NWA	0.81	28	13	0.27	3698	867	0.64	41	9	0.27	3679	455
SA	0.08	6	4	0.18	4103	429	-0.14	3	2	0.11	4533	120
SEA	0.63	13	12	0.26	3306	787	0.55	14	14	0.23	3163	799
SWA	0.96	6	4	0.32	2302	929	0.51	2	2	0.12	4156	172
I	0.23	6	4	0.26	2287	529	0.06	4	4	0.19	2347	581
NP	0.03	14	7	0.20	2015	448	-0.10	9	8	0.24	2815	673
SP	0.45	12	5	0.30	2285	924	0.06	3	3	0.15	2724	709

### 3.2 Volume-weighted regional $\delta^{13}\text{C}$

200 The second approach we use to further constrain the LIG-Holocene  $\delta^{13}\text{C}$  anomaly is to estimate the volume-weighted regional  $\delta^{13}\text{C}$ . We define our regional boundaries based on the regions described in Peterson et al. (2014), however we only include the regions where there is enough data to justify an analysis. For all the data in each of these regions, we calculate a mean value by taking the direct averages of all data. We divide the ocean basins into eight regions (Table 4, shown in Fig. 2) and calculate the volume-weighted averages  $\delta^{13}\text{C}$  for each of these regions. Since the Atlantic and Pacific Oceans have more data than the  
205 Indian Ocean, there is greater confidence in the  $\delta^{13}\text{C}$  estimates for these regions. These regional averages are then used to calculate a global volume-weighted  $\delta^{13}\text{C}$ .

Results for the Atlantic and Pacific Oceans are given in Fig. 6, and show a mean LIG-Holocene anomaly of -0.21 ‰ and -0.27 ‰ respectively, slightly higher than the range of estimates for the four regions selected in Sect. 3.1. There is a higher offset estimated in this definition of the southwest Atlantic (-0.45 ‰) than in Sect. 3.1, however there are only 4 cores available  
210 in this region during the Holocene and 2 during the LIG.

The estimated LIG-Holocene anomaly in the south Pacific is relatively high at -0.39 ‰, giving a relatively large Pacific anomaly estimate of -0.27 ‰. This could be due in part to the deeper location of the LIG cores compared to the mean of the Holocene cores (439 m difference, Table 4). There is less confidence in the estimate of the Pacific volume-weighted mean since the proxy data is sparse, and the majority of cores are from the eastern equatorial Pacific as shown in Fig. 2. We also note  
215 that the average depths of cores from the Pacific Ocean (LIG: 2,711 m, Holocene: 2,131 m) and Indian Ocean (LIG: 2,383 m, Holocene: 2,303 m) are shallower than that of the Atlantic Ocean (LIG: 3,531 m, Holocene: 3,157 m; Fig. 3). However, as the vertical gradient below 2,000 m depth in the Pacific Ocean is small (e.g. Eide et al., 2017), this might not significantly impact our results.

There is a small positive trend in the average Atlantic  $\delta^{13}\text{C}$  from 125 ka BP, reaching a maximum value at 118 ka BP (Fig.  
220 6). The average core depth over the 125–120 ka BP time period does not suggest that a change in the mean depth could explain

this variation. Fitting a linear regression over this period indicates an increase in  $\delta^{13}\text{C}$  of  $0.03\text{‰ ka}^{-1}$  in the Atlantic, with a p-value of 0.01 and an  $R^2$  of 0.85 (Fig. 4a). For the Pacific, there is a  $\sim 0.13\text{‰}$  increase in  $\delta^{13}\text{C}$  between 7 and 5 ka BP, which could be associated with the early Holocene terrestrial regrowth (Menviel and Joos, 2012).

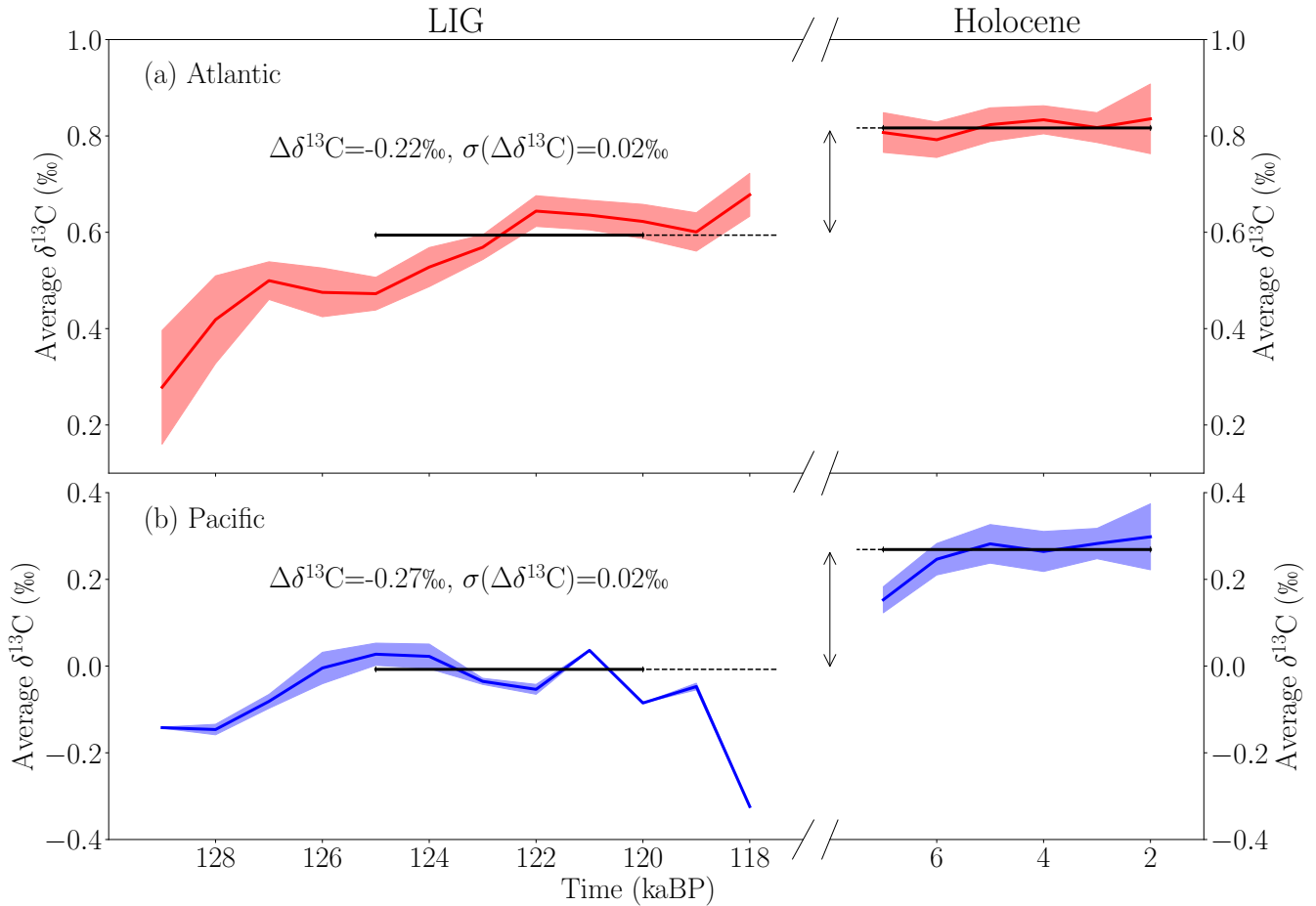


**Figure 6.** Comparison of volume-weighted  $\delta^{13}\text{C}$  for the Atlantic (red) and Pacific (blue) for the LIG and Holocene, calculated using the regions from Peterson et al. (2014) from data covering all depths. Solid coloured lines indicate the mean volume-weighted  $\delta^{13}\text{C}$ , and the shading indicates the volume-weighted sum of square deviations from the mean. The horizontal bars indicate the mean of the stable period determined from the regional analysis as defined in Sect. 3.1 (LIG: 125–120 ka BP, Holocene: 7–2 ka BP), with the  $\Delta\delta^{13}\text{C}$  indicating the mean anomaly between these two average and the standard deviation ( $\sigma(\delta^{13}\text{C}), \text{‰}$ ).

For the Indian Ocean, we only include four cores, as these are the only ones spanning both the LIG and Holocene. An LIG  
225 anomaly of  $-0.13\text{‰}$  in the Indian Ocean compared to the Holocene is therefore associated with higher uncertainties. The whole ocean mean LIG  $\delta^{13}\text{C}$  anomaly is  $-0.25\text{‰}$ , but it is associated with higher uncertainties than each region anomaly.

Both the regional analysis of our new database and our volume-weighted estimate indicate that the global mean  $\delta^{13}\text{C}$  was about 0.2 ‰ lower during the LIG than during the Holocene. We further test the robustness of this result in the next section.

### 3.3 Reconstruction of the LIG Atlantic Meridional Overturning Circulation

In this section, we analyse the spatial  $\delta^{13}\text{C}$  distribution in the Atlantic Ocean to assess potential changes in the penetration depth and southward expansion of NADW during the LIG, defined here as 125–120 ka BP, with respect to the Holocene. A change in NADW might influence our estimate of the mean  $\delta^{13}\text{C}$ , given that most of the available data is localised in the Atlantic Ocean.

We use simple statistical regression models to reconstruct NADW and AABW separately with a quadratic-with-depth and linear-with-latitude equation following the method of Bengtson et al. (2019). For consistency, the regression algorithm only includes records from cores that span both the LIG and Holocene and uses a weighted least squares approach, where the weighting equals the number of samples per core. The modelled region is defined between 40° S and 60° N as this is the region where we can expect to find both the NADW and AABW  $\delta^{13}\text{C}$  signals.

The results are shown in Fig. 7. We test the robustness of our statistical model using the jackknifing technique. We systematically exclude each individual core from the database one at a time, fit the parameters using this modified database, and compare the model prediction against the core which was excluded. This produces small variations in the average mean response of the statistical models (the standard deviations were 0.01 ‰ for both the LIG and Holocene, respectively).

We calculate end-member values based on proxies located near the water mass sources. These are taken as 0.79 ‰ and 1.02 ‰ for NADW for the LIG and Holocene, respectively, and -0.09 ‰ and 0.23 ‰ for AABW for the LIG and Holocene, respectively. The end-member values are calculated as the average of cores shallower than 3,000 m but deeper than 1,000 m and located between 50° N and 70° N for NADW. The NADW end-member cores have an average depth of 2,043 m and a standard deviation of 478 m during the LIG. For the AABW end-member, the only eligible core is ODP1089, which is at ~41° S and 4,621 m.

The mean volume-weighted  $\delta^{13}\text{C}$  for the Atlantic Ocean between 40° S and 60° N based on this interpolation is 0.53 ‰ for the LIG and 0.70 ‰ for the Holocene (Fig. 7). This suggests a 0.17 ‰ lower Atlantic  $\delta^{13}\text{C}$  at the LIG than the Holocene. Our statistical reconstruction points to a very similar NADW depth (~2,600 m) for both time periods (Fig. 7). The NADW depth is defined here as the depth of maximum  $\delta^{13}\text{C}$  in the North Atlantic.

We also investigate the meridional gradient in  $\delta^{13}\text{C}$  in the Atlantic Ocean to determine whether the NADW southward penetration, transport and remineralisation rates were significantly different during the LIG compared to the Holocene. We only consider cores that are located between depths of 1,000 and 3,000 m in order to stay within the main pathway of NADW (Fig. 8a). Though there is significant scatter, in accordance with our previous findings, a moving average through the Holocene and the LIG data shows that LIG  $\delta^{13}\text{C}$  is typically lower than the Holocene counterparts. However, the meridional  $\delta^{13}\text{C}$  statistical model gradients are not very different for the LIG ( $0.0036 \text{ ‰ } \text{latitude}^{-1}$ ) and the Holocene ( $0.0030 \text{ ‰ } \text{latitude}^{-1}$ ) (Fig. 8a), suggesting a similar southward penetration of NADW.

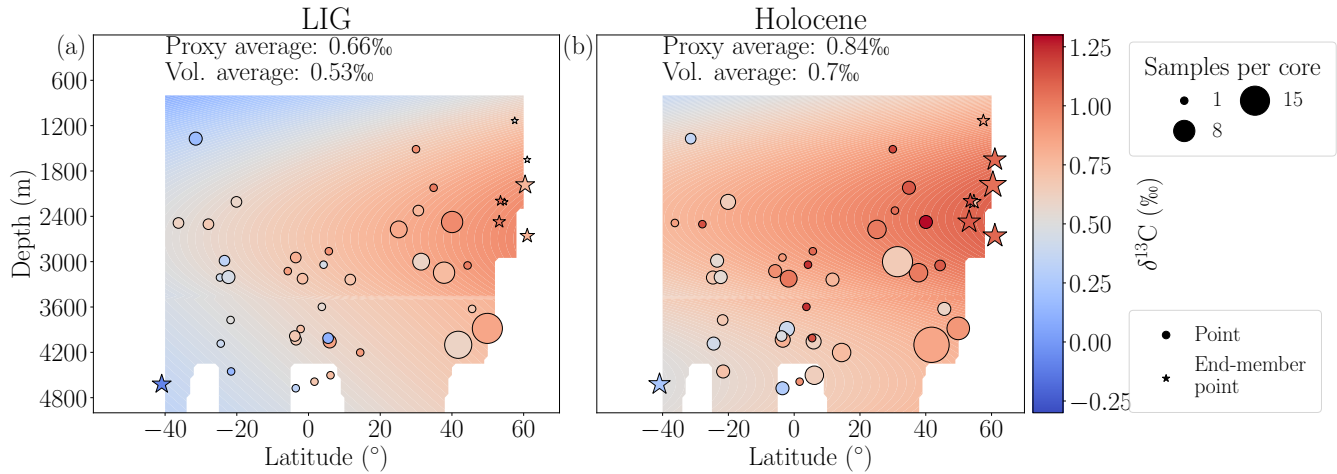


**Figure 7.** Reconstructed Atlantic  $\delta^{13}\text{C}$  ( $\text{\textperthousand}$ ) meridional section during the LIG (125–120 ka BP) and Holocene (7–2 ka BP). The circular points represent the proxy data, showing the average  $\delta^{13}\text{C}$  with colour and the number of points per core with size. The stars represent the proxy data which make up the end-members. Background shading shows the reconstructed  $\delta^{13}\text{C}$  using a quadratic statistical regression of the proxy data following the method described in Bengtson et al. (2019).

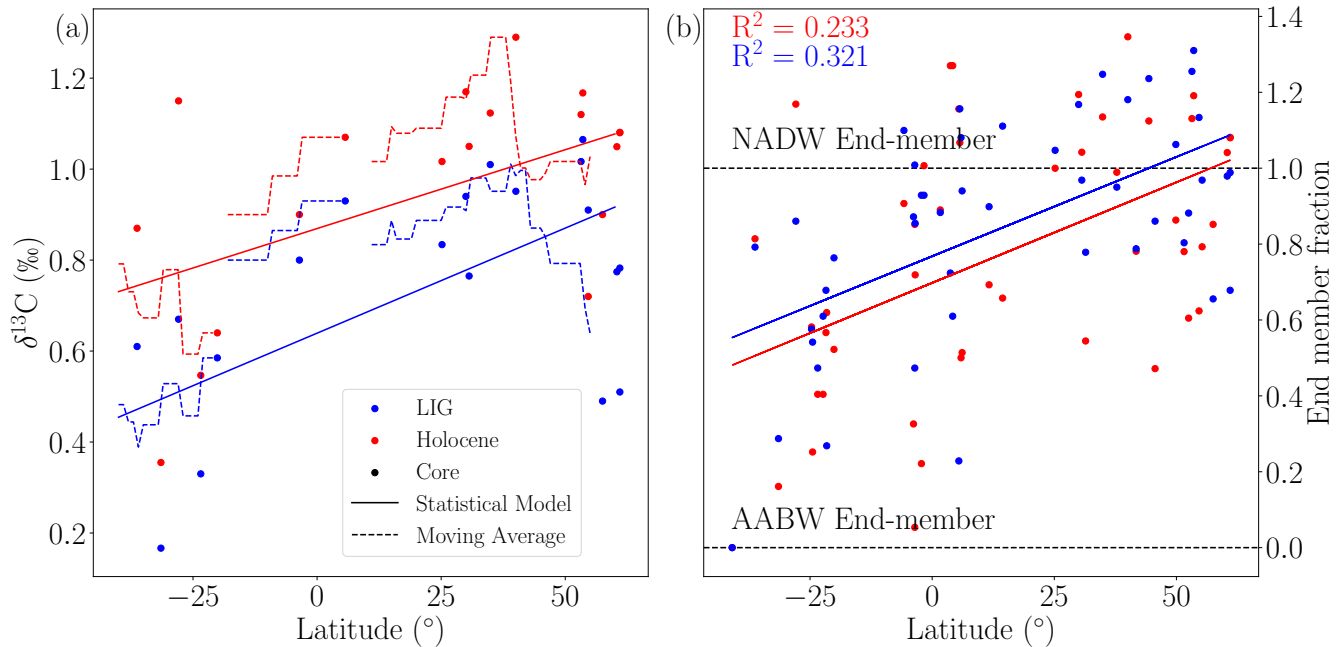


**Figure 8.** The meridional gradient of the Atlantic Ocean benthic  $\delta^{13}\text{C}$  ( $\text{\textperthousand}$ ). a) Holocene (red) and LIG (blue)  $\delta^{13}\text{C}$  for each core (points) between 1,000 m and 3,000 m. Dotted lines are the moving averages of the cores. Solid lines indicate the results of our statistical model at 2,000 m. b) Average  $\delta^{13}\text{C}$  for each record deeper than 1,000 m as a proportion of the end-members. A value of one indicates the NADW end-member and a value of zero the AABW end-member. Solid lines show the linear regressions of the records.

260 Using  $\delta^{13}\text{C}$  of the end-members for NADW and AABW, we use a simple binary mixing model for all cores deeper than 1,000 m to estimate changes in NADW penetration (Fig. 8b). The LIG and Holocene  $\delta^{13}\text{C}$  slopes in the Atlantic are similar, indicating similar southward penetration of NADW during both time periods. This suggests that the differences in  $\delta^{13}\text{C}$  between the two time periods is most likely due to change in end-member values, while the mean Atlantic oceanic circulation was likely similar.

265 Based on our analysis, there appears to be no significant difference in the mean time-averaged AMOC between the LIG and the Holocene. Negative LIG-Holocene anomalies are found for each of the smaller regions selected (northeast Atlantic, equatorial Atlantic, southeast Atlantic, and eastern equatorial Pacific), with statistical significance seen in all regions except the equatorial Atlantic, where an unusual low  $\delta^{13}\text{C}$  value in one core is responsible for narrowing the difference between the two period means. Additionally, our volume-weighted mean  $\delta^{13}\text{C}$  estimates have similar anomalies in the Atlantic and Pacific Oceans (-0.21 ‰ and -0.27 ‰ respectively, Fig. 6).

270 **4 Discussion**

One of the goals of our study is to assess the mean change in oceanic  $\delta^{13}\text{C}$  between the LIG and the Holocene. Given the uncertainties in the chronologies, avoiding data that pertains to deglaciation, and capturing the same length of time during the LIG and the Holocene, we chose the periods 125 to 120 ka BP for the LIG and 7 to 2 ka BP for the Holocene. Using a similar geographical distribution of data points for both periods, we find that the oceanic  $\delta^{13}\text{C}$  was ~0.2 ‰ lower during the LIG than

275 the Holocene.

Our analysis of the  $\delta^{13}\text{C}$  signal suggests consistent LIG-Holocene  $\delta^{13}\text{C}$  anomalies in different regions of the Atlantic basins, as well as in the Pacific and Indian Oceans, even if there are significant uncertainties with the later due to fewer available records. The  $\delta^{13}\text{C}$  distribution in the Atlantic Ocean suggests that there was no significant mean change in the southward penetration or depth of NADW during the LIG (125–120 ka BP) compared to the Holocene (7–2 ka BP). A statistical reconstruction

280 of the early LIG (128–123 ka BP)  $\delta^{13}\text{C}$  compared to our 125–120 ka BP reconstruction does not reveal a significant difference in either the NADW core depth or NADW extent as indicated by the meridional  $\delta^{13}\text{C}$  gradients (Fig. S2). The volume weighted average  $\delta^{13}\text{C}$  during the early LIG is 0.06 ‰ lighter than during the LIG period considered here (125–120 ka BP). Since both time slices (128–123 ka BP and 125–120 ka BP) are 5 ka averages and include dating uncertainties of ~2 ka, it is not possible to resolve potential centennial-scale oceanic circulation changes (e.g. Galaasen et al., 2014b; Tzedakis et al., 2018).

285 Explanations for the 0.2 ‰ lower  $\delta^{13}\text{C}$  anomaly in the ocean may include a redistribution between the ocean-atmosphere system. Such a redistribution can result from a change in end-member values (Fig. 8). As fractionation during air-sea gas exchange is temperature dependent, globally higher SSTs at the LIG could lead to a lower oceanic  $\delta^{13}\text{C}$ . However, the effect of this is likely small (Brovkin et al., 2002) and would also lead to a higher atmospheric  $\delta^{13}\text{CO}_2$  at the LIG, which is inconsistent with Antarctic ice core measurements that suggest an anomaly of -0.3 ‰ (Schneider et al., 2013). Lower nutrient utilisation in

290 the North Atlantic would decrease surface ocean  $\delta^{13}\text{C}$  and thus the  $\delta^{13}\text{C}$  end-members. However, this would also imply that less organic carbon would be remineralised at depth. Therefore, it is unlikely that the lower average oceanic mean  $\delta^{13}\text{C}$  results from a change in end-members through lower surface ocean nutrient utilisation. Currently, there is still a lack of constraints on

nutrient utilisation in these end-member regions during the LIG compared to the Holocene. Therefore, the lower  $\delta^{13}\text{C}$  in the ocean-atmosphere system cannot be explained by a simple redistribution of  $\delta^{13}\text{C}$  between the atmosphere and the ocean.

An alternative explanation for the anomaly is a change in the terrestrial carbon storage, which has a typical signature of approximately -37 to -20 ‰ for C3 derived plant material (Kohn, 2010) and -13 ‰ for C4 derived plant material (Basu et al., 2015). The total land carbon content at the LIG is poorly constrained. Proxies generally suggest extensive vegetation during the LIG compared to the Holocene (CAPE, 2006; Govin et al., 2015; Larrasoña et al., 2013; Muhs et al., 2001; Tarasov et al., 2005; de Vernal and Hillaire-Marcel, 2008), which would imply a greater land carbon store. However, other terrestrial carbon stores including peatlands and permafrost may also have differed during the LIG compared to the Holocene. With an estimated ~550 Gt C stored in peats today (mean  $\delta^{13}\text{C}$  ~-28 ‰, Dioumaeva et al. (2002); Novák et al. (1999)) and ~1,000 Gt C in the active layer in permafrost, which may have been partially thawed during the LIG (Reyes et al., 2010; Schuur et al., 2015; Stapel et al., 2018), less carbon stored in peat and permafrost at the LIG could have led to a lower total land carbon store compared to the Holocene. However, it is not possible to infer this total land carbon change from the oceanic and atmospheric  $\delta^{13}\text{C}$  anomalies because it cannot be assumed that the mass of carbon and  $^{13}\text{C}$  is preserved within the ocean-atmosphere-land biosphere system on glacial-interglacial timescales. There is indeed continuous exchange of carbon and  $^{13}\text{C}$  between the lithosphere and the coupled ocean, atmosphere and land biosphere carbon reservoirs. Isotopic perturbations associated with changes in the terrestrial biosphere are communicated to the burial fluxes of organic carbon and  $\text{CaCO}_3$  and are therefore attenuated on multi-millennial time scales (Jeltsch-Thömmes et al., 2019; Jeltsch-Thömmes and Joos, 2020). Nevertheless, when hypothetically neglecting any exchange with the lithosphere, we find that the change in terrestrial carbon needed to explain the difference in  $\delta^{13}\text{C}$  would be in the order of  $310 \pm 44$  Gt C less during the LIG than the Holocene (Text S1).

In addition, due to the warmer conditions at the LIG than during the Holocene, there could have been a release of methane clathrates which would have added isotopically light carbon ( $\delta^{13}\text{C}$ : ~-47 ‰) to the ocean-atmosphere system. However, available evidence suggests that geological  $\text{CH}_4$  sources are rather small (Bock et al., 2017; Dyonisius et al., 2020; Hmiel et al., 2020; Saunois et al., 2020) making this explanation unlikely, although we cannot completely exclude the possibility that the geological  $\text{CH}_4$  source was larger at the LIG than the Holocene. Similarly, since  $\delta^{13}\text{CO}_2$  from volcanic outgassing has a similar value to atmospheric  $\delta^{13}\text{CO}_2$  (Brovkin et al., 2016) and modelling suggests volcanic outgassing likely only had a minor impact on  $\delta^{13}\text{CO}_2$  (Roth and Joos, 2012), it is unlikely that volcanic outgassing of  $\text{CO}_2$  played a significant role in influencing the mean oceanic  $\delta^{13}\text{C}$ .

While changes in terrestrial carbon could have impacted the oceanic  $\delta^{13}\text{C}$  at the LIG, the LIG-Holocene differences in the isotopic signal of both the atmosphere and ocean were most likely due to a long-term imbalance between the isotopic fluxes to and from the lithosphere, including the net burial (or redissolution) of organic carbon and  $\text{CaCO}_3$  in deep-sea sediments, and changes in shallow water sedimentation and coral reef formation (Jeltsch-Thömmes and Joos, 2020).

## 5 Conclusions

325 We present a new compilation of benthic  $\delta^{13}\text{C}$  from 130 to 115 ka BP covering the LIG. Over this time period, benthic  $\delta^{13}\text{C}$  generally display a maximum value at  $\sim 121$  ka BP ( $\pm 2$  ka), in phase with the maximum atmospheric  $\delta^{13}\text{CO}_2$  (LIG value of  $-6.5\text{ ‰}$  at  $\sim 120$  ka BP). As there are significant chronological uncertainties associated with LIG records, we analyse data between 125 and 120 ka BP to avoid data associated with millennial-scale events and the deglaciation. We compare this LIG benthic  $\delta^{13}\text{C}$  data to a similar database covering the Holocene (7–2 ka BP). We find that during these specific time periods, 330 LIG oceanic  $\delta^{13}\text{C}$  was about  $0.2\text{ ‰}$  lower than during the Holocene. This anomaly is consistent across different regions in the Atlantic Ocean. Even though there are less records available, benthic  $\delta^{13}\text{C}$  data from the Pacific Ocean also support an anomaly of about  $0.2\text{ ‰}$ .

An analysis of  $\delta^{13}\text{C}$  gradients across the Atlantic Ocean suggests that there were no significant changes in mean, long-term ocean circulation between the two intervals. While reduced high northern latitude peat and permafrost caused by higher 335 temperatures at the LIG than during the Holocene (Otto-Bliesner et al., 2020) could have lead to a lower atmospheric and oceanic  $\delta^{13}\text{C}$ , the most likely explanation for the lower LIG oceanic  $\delta^{13}\text{C}$  is a long term imbalance in the weathering and burial of carbon. Additional studies are required to further constrain the LIG carbon balance.

*Data availability.* The data is published on Research Data Australia at DOI <https://doi.org/10.26190/5efe841541f3b>.

*Author contributions.* SAB, LCM, and KJM designed the research. CDP and LEL provided significant portions of the  $\delta^{13}\text{C}$  data. SAB, 340 LCM, KJM, and LM analysed the data and developed the methodology. FJ assisted in the interpretation of the results. SAB prepared the manuscript with contributions from all co-authors.

*Competing interests.* The authors declare that they have no conflict of interest.

*Acknowledgements.* Shannon Bengtson acknowledges funding from the Australian Government Research Training Program Scholarship. Laurie Menviel and Katrin Meissner acknowledge funding from the Australian Research Council grants FT180100606 (to Laurie Menviel) 345 and DP180100048 (to Katrin Meissner and Laurie Menviel). Computational resources were provided by the NCI National Facility at the Australian National University through awards under the Merit Allocation Scheme, the Intersect allocation scheme, and the UNSW HPC at NCI Scheme. Fortunat Joos acknowledges funding from the Swiss National Science Foundation (#200020\_172476). This study was facilitated by the PAGES QUIGS working group.

## References

- 350 Alley, R. B. and Ágústsdóttir, A. M.: The 8k event: cause and consequences of a major Holocene abrupt climate change, Quaternary Science Reviews, 24, 1123–1149, <https://doi.org/10.1016/j.quascirev.2004.12.004>, <http://www.sciencedirect.com/science/article/pii/S0277379105000314>, 2005.
- Anderson, R. S., Jiménez-Moreno, G., Ager, T., and Porinchu, D. F.: High-elevation paleoenvironmental change during MIS 6–4 in the central Rockies of Colorado as determined from pollen analysis, Quaternary Research, 82, 542–552, <https://doi.org/10.1016/j.yqres.2014.03.005>,  
355 <http://www.sciencedirect.com/science/article/pii/S0033589414000398>, 2014.
- Axford, Y., Briner, J., R. Francis, D., H. Miller, G., R. Walker, I., and Wolfe, A.: Chironomids record terrestrial temperature changes throughout Arctic interglacials of the past 200,000 yr, Geological Society of America Bulletin, 123, 1275–1287, <https://doi.org/10.1130/B30329.1>, 2011.
- Bakker, P., Stone, E. J., Charbit, S., Gröger, M., Krebs-Kanzow, U., Ritz, S. P., Varma, V., Khon, V., Lunt, D. J., Mikolajewicz, U., Prange, M., Renssen, H., Schneider, B., and Schulz, M.: Last interglacial temperature evolution – a model inter-comparison, Climate of the Past, 9, 605–619, <https://doi.org/https://doi.org/10.5194/cp-9-605-2013>, <https://www.clim-past.net/9/605/2013/>, 2013.
- 360 Basu, S., Agrawal, S., Sanyal, P., Mahato, P., Kumar, S., and Sarkar, A.: Carbon isotopic ratios of modern C3–C4 plants from the Gangetic Plain, India and its implications to paleovegetational reconstruction, Palaeogeography Palaeoclimatology Palaeoecology, 440, <https://doi.org/10.1016/j.palaeo.2015.08.012>, 2015.
- 365 Bazin, L., Landais, A., Lemieux-Dudon, B., Toyé Mahamadou Kele, H., Veres, D., Parrenin, F., Martinerie, P., Ritz, C., Capron, E., Lipenkov, V. Y., Loutre, M.-F., Raynaud, D., Vinther, B. M., Svensson, A. M., Rasmussen, S. O., Severi, M., Blunier, T., Leuenberger, M. C., Fischer, H., Masson-Delmotte, V., Chappellaz, J. A., and Wolff, E. W.: delta Deuterium measured on ice core EDC on AICC2012 chronology, In: Bazin, L et al. (2013): The Antarctic ice core chronology (AICC2012). PANGAEA, <https://doi.org/10.1594/PANGAEA.824894>, <https://doi.org/10.1594/PANGAEA.824891>, <https://doi.pangaea.de/10.1594/PANGAEA.824891>, 2013.
- 370 Belanger, P. E., Curry, W. B., and Matthews, R. K.: Core-top evaluation of benthic foraminiferal isotopic ratios for paleo-oceanographic interpretations, Palaeogeography, Palaeoclimatology, Palaeoecology, 33, 205–220, [https://doi.org/10.1016/0031-0182\(81\)90039-0](https://doi.org/10.1016/0031-0182(81)90039-0), <http://www.sciencedirect.com/science/article/pii/0031018281900390>, 1981.
- Bengtson, S. A., Meissner, K. J., Men viel, L., A. Sisson, S., and Wilkin, J.: Evaluating the extent of North Atlantic Deep Water and the mean Atlantic  $\delta^{13}\text{C}$  from statistical reconstructions, Paleoceanography and Paleoclimatology, <https://doi.org/10.1029/2019PA003589>, 2019.
- 375 Bereiter, B., Eggleston, S., Schmitt, J., Nehrbass-Ahles, C., Stocker, T. F., Fischer, H., Kipfstuhl, S., and Chappellaz, J.: Revision of the EPICA Dome C CO<sub>2</sub> record from 800 to 600 kyr before present, Geophysical Research Letters, 42, 542–549, <https://doi.org/10.1002/2014GL061957>, <https://agupubs.onlinelibrary.wiley.com/doi/abs/10.1002/2014GL061957>, 2015.
- Bickert, T. and Mackensen, A.: Last Glacial to Holocene Changes in South Atlantic Deep Water Circulation, in: The South Atlantic in the Late Quaternary: Reconstruction of Material Budgets and Current Systems, edited by Wefer, G., Multizta, S., and Ratmeyer, V., pp. 380 671–693, Springer, Berlin, Heidelberg, [https://doi.org/10.1007/978-3-642-18917-3\\_29](https://doi.org/10.1007/978-3-642-18917-3_29), 2003.
- Bickert, T. and Wefer, G.: Late Quaternary Deep Water Circulation in the South Atlantic: Reconstruction from Carbonate Dissolution and Benthic Stable Isotopes, in: The South Atlantic: Present and Past Circulation, edited by Wefer, G., Berger, W. H., Siedler, G., and Webb, D. J., pp. 599–620, Springer, Berlin, Heidelberg, [https://doi.org/10.1007/978-3-642-80353-6\\_30](https://doi.org/10.1007/978-3-642-80353-6_30), 1996.
- Bickert, T., Curry, W. B., and Wefer, G.: Late Pliocene to Holocene (2.6 – 0 Ma) western equatorial Atlantic deep-water circulation: inferences  
385 from benthic stable isotopes, vol. 154, pp. 239–254, Proc. Ocean Drill. Program Sci. Results, 1997.

- Bickert, T., Wefer, G., and Müller, P. J.: Stable isotopes and sedimentology of core GeoB1032-2, PANGAEA, <https://doi.org/10.1594/PANGAEA.103613>, <https://doi.pangaea.de/10.1594/PANGAEA.103613>, 2003.
- Bock, M., Schmitt, J., Beck, J., Seth, B., Chappellaz, J., and Fischer, H.: Glacial/interglacial wetland, biomass burning, and geologic methane emissions constrained by dual stable isotopic CH<sub>4</sub> ice core records, *Proceedings of the National Academy of Sciences*, 114, E5778–E5786, 390 <https://doi.org/10.1073/pnas.1613883114>, <https://www.pnas.org/content/114/29/E5778>, 2017.
- Böhm, E., Lippold, J., Gutjahr, M., Frank, M., Blaser, P., Antz, B., Fohlmeister, J., Frank, N., Andersen, M. B., and Deininger, M.: Strong and deep Atlantic meridional overturning circulation during the last glacial cycle, *Nature*, 517, 73–76, <https://doi.org/10.1038/nature14059>, <https://www.nature.com/articles/nature14059>, 2015.
- Boyle, E. A.: Cadmium and δ<sup>13</sup>C Paleochemical Ocean Distributions During the Stage 2 Glacial Maximum, *Annual Review of Earth and Planetary Sciences*, 20, 245–287, <https://doi.org/10.1146/annurev.ea.20.050192.001333>, <https://www.annualreviews.org/doi/10.1146/annurev.ea.20.050192.001333>, 1992.
- Boyle, E. A. and Keigwin, L.: North Atlantic thermohaline circulation during the past 20,000 years linked to high-latitude surface temperature, *Nature*, 330, 35–40, <https://doi.org/10.1038/330035a0>, <https://www.nature.com/articles/330035a0>, 1987.
- Boyle, E. A. and Keigwin, L. D.: Comparison of Atlantic and Pacific paleochemical records for the last 215,000 years: changes in deep ocean 400 circulation and chemical inventories, *Earth and Planetary Science Letters*, 76, 135–150, [https://doi.org/10.1016/0012-821X\(85\)90154-2](https://doi.org/10.1016/0012-821X(85)90154-2), <http://www.sciencedirect.com/science/article/pii/0012821X85901542>, 1985.
- Brovkin, V., Bendtsen, J., Claussen, M., Ganopolski, A., Kubatzki, C., Petoukhov, V., and Andreev, A.: Carbon cycle, vegetation, and climate dynamics in the Holocene: Experiments with the CLIMBER-2 model, *Global Biogeochemical Cycles*, 16, 86–1–86–20, <https://doi.org/10.1029/2001GB001662>, <https://agupubs.onlinelibrary.wiley.com/doi/abs/10.1029/2001GB001662>, 2002.
- Brovkin, V., Brücher, T., Kleinen, T., Zaehle, S., Joos, F., Roth, R., Spahni, R., Schmitt, J., Fischer, H., Leuenberger, M., Stone, E. J., Ridgwell, A., Chappellaz, J., Kehrwald, N., Barbante, C., Blunier, T., and Dahl Jensen, D.: Comparative carbon cycle dynamics of the present and last interglacial, *Quaternary Science Reviews*, 137, 15–32, <https://doi.org/10.1016/j.quascirev.2016.01.028>, <http://www.sciencedirect.com/science/article/pii/S0277379116300300>, 2016.
- Cane, R. E., Oppo, D. W., and Curry, W. B.: Atlantic Ocean circulation during the Younger Dryas: Insights from a new Cd/Ca record 410 from the western subtropical South Atlantic, *Paleoceanography*, 18, <https://doi.org/10.1029/2003PA000888>, <https://agupubs.onlinelibrary.wiley.com/doi/abs/10.1029/2003PA000888>, 2003.
- Candy, S. and Alonso-Garcia, M.: Sea surface temperature reconstruction for sediment core GIK23414-6, PANGAEA, <https://doi.org/10.1594/PANGAEA.894428>, <https://doi.pangaea.de/10.1594/PANGAEA.894428>, 2018.
- CAPE: Last Interglacial Arctic warmth confirms polar amplification of climate change, *Quaternary Science Reviews*, 25, 1383–1400, 415 <https://doi.org/10.1016/j.quascirev.2006.01.033>, <http://www.sciencedirect.com/science/article/pii/S0277379106000990>, 2006.
- Cernusak, L. A., Ubierna, N., Winter, K., Holtum, J. A. M., Marshall, J. D., and Farquhar, G. D.: Environmental and physiological determinants of carbon isotope discrimination in terrestrial plants, *New Phytologist*, 200, 950–965, <https://doi.org/10.1111/nph.12423>, <https://nph.onlinelibrary.wiley.com/doi/abs/10.1111/nph.12423>, 2013.
- Chapman, M. and Shackleton, N.: Late Quaternary North Atlantic IRD and Isotope Data, IGBP PAGES/World Data Center for Paleoclimatology, 420 1999.
- Chen, J., Farrell, J. W., Murray, D. W., and Prell, W. L.: Timescale and paleoceanographic implications of a 3.6 m.y. oxygen isotope record from the northeast Indian Ocean (Ocean Drilling Program Site 758), *Paleoceanography*, 10, 21–47, <https://doi.org/10.1029/94PA02290>, <https://agupubs.onlinelibrary.wiley.com/doi/abs/10.1029/94PA02290>, 1995.

- Cheng, X., Tian, J., and Wang, P.: Stable isotopes from Site 1143, Tech. Rep. 184, International Ocean Discovery Program, 2004.
- 425 Collins, J. A., Schefuß, E., Heslop, D., Mulitza, S., Prange, M., Zabel, M., Tjallingii, R., Dokken, T. M., Huang, E., Mackensen, A., Schulz, M., Tian, J., Zarriess, M., and Wefer, G.: Interhemispheric symmetry of the tropical African rainbelt over the past 23,000 years, *Nature Geoscience*, 4, 42–45, <https://doi.org/10.1038/ngeo1039>, <http://adsabs.harvard.edu/abs/2011NatGe...4...42C>, 2011.
- Cortijo, E.: Stable isotope analysis on sediment core SU90-39, PANGAEA, <https://doi.org/https://doi.org/10.1594/PANGAEA.106761>, <https://doi.pangaea.de/10.1594/PANGAEA.106761>, 2003.
- 430 Curry, W., Shackleton, N., and Richter, C.: Proc. ODP, Init. Repts, 154: College Station, TX (Ocean Drilling Program), <https://doi.org/10.2973/odp.proc.ir.154.1995>, 1995.
- Curry, W. B. and Lohmann, G. P.: Carbon isotopic changes in benthic foraminifera from the western South Atlantic: Reconstruction of glacial abyssal circulation patterns, *Quaternary Research*, 18, 218–235, [https://doi.org/10.1016/0033-5894\(82\)90071-0](https://doi.org/10.1016/0033-5894(82)90071-0), <http://www.sciencedirect.com/science/article/pii/0033589482900710>, 1982.
- 435 Curry, W. B. and Oppo, D. W.: Synchronous, high-frequency oscillations in tropical sea surface temperatures and North Atlantic Deep Water production during the Last Glacial Cycle, *Paleoceanography*, 12, 1–14, <https://doi.org/10.1029/96PA02413>, <https://agupubs.onlinelibrary.wiley.com/doi/abs/10.1029/96PA02413>, 1997.
- Curry, W. B. and Oppo, D. W.: Glacial water mass geometry and the distribution of  $\delta^{13}\text{C}$  of  $\Sigma\text{CO}_2$  in the western Atlantic Ocean, *Paleoceanography*, 20, <https://doi.org/10.1029/2004PA001021>, <https://agupubs.onlinelibrary.wiley.com/doi/abs/10.1029/2004PA001021>, 2005.
- 440 Curry, W. B., Duplessy, J. C., Labeyrie, L., and Shackleton, N. J.: Changes in the distribution of  $\delta^{13}\text{C}$  of deep water  $\Sigma\text{CO}_2$  between the Last Glaciation and the Holocene, *Paleoceanography*, 3, 317–341, <https://doi.org/10.1029/PA003i003p00317>, <https://agupubs.onlinelibrary.wiley.com/doi/abs/10.1029/PA003i003p00317>, 1988.
- de Abreu, L., Shackleton, N. J., Schönfeld, J., Hall, M., and Chapman, M.: Millennial-scale oceanic climate variability off the Western Iberian margin during the last two glacial periods, *Marine Geology*, 196, 1–20, [https://doi.org/10.1016/S0025-3227\(03\)00046-X](https://doi.org/10.1016/S0025-3227(03)00046-X), <http://www.sciencedirect.com/science/article/pii/S002532270300046X>, 2003.
- 445 de Vernal, A. and Hillaire-Marcel, C.: Natural Variability of Greenland Climate, Vegetation, and Ice Volume During the Past Million Years, *Science*, 320, 1622–1625, <https://doi.org/10.1126/science.1153929>, <https://science.scienmag.org/content/320/5883/1622>, 2008.
- Deaney, E. L., Barker, S., and van de Flierdt, T.: Timing and nature of AMOC recovery across Termination 2 and magnitude of deglacial CO<sub>2</sub> change, *Nature Communications*, 8, 1–10, <https://doi.org/10.1038/ncomms14595>, <https://www.nature.com/articles/ncomms14595>, 2017.
- 450 Diefendorf, A. F. and Freimuth, E. J.: Extracting the most from terrestrial plant-derived n-alkyl lipids and their carbon isotopes from the sedimentary record: A review, *Organic Geochemistry*, 103, 1–21, <https://doi.org/10.1016/j.orggeochem.2016.10.016>, <http://www.sciencedirect.com/science/article/pii/S014663801630287X>, 2017.
- Diefendorf, A. F., Mueller, K. E., Wing, S. L., Koch, P. L., and Freeman, K. H.: Global patterns in leaf  $^{13}\text{C}$  discrimination and implications for studies of past and future climate, *Proceedings of the National Academy of Sciences*, 107, 5738–5743, <https://doi.org/10.1073/pnas.0910513107>, <https://www.pnas.org/content/107/13/5738>, 2010.
- 455 Dioumaeva, I., Trumbore, S., Schuur, E. A. G., Goulden, M. L., Litvak, M., and Hirsch, A. I.: Decomposition of peat from upland boreal forest: Temperature dependence and sources of respiration carbon, *Journal of Geophysical Research: Atmospheres*, 107, WFX 3–1–WFX 3–12, <https://doi.org/10.1029/2001JD000848>, <https://agupubs.onlinelibrary.wiley.com/doi/abs/10.1029/2001JD000848>, 2002.
- Drake, N. A., Blench, R. M., Armitage, S. J., Bristow, C. S., and White, K. H.: Ancient watercourses and biogeography of the Sahara explain the peopling of the desert, *Proceedings of the National Academy of Sciences*, 108, 458–462, <https://doi.org/10.1073/pnas.1012231108>, <https://www.pnas.org/content/108/2/458>, 2011.

- Duplessy, J.: Quaternary paleoceanography: unpublished stable isotope records. IGBP PAGES/World Data Center for Paleoclimatology Data Contribution Series: #1996-035., Tech. rep., NOAA/NGDC Paleoclimatology Program, Boulder, Colorado, USA, 1996.
- Duplessy, J.-C., Shackleton, N. J., Matthews, R. K., Prell, W., Ruddiman, W. F., Caralp, M., and Hendy, C. H.:  $^{13}\text{C}$  Record of benthic foraminifera in the last interglacial ocean: Implications for the carbon cycle and the global deep water circulation, *Quaternary Research*, 21, 225–243, [https://doi.org/10.1016/0033-5894\(84\)90099-1](https://doi.org/10.1016/0033-5894(84)90099-1), <http://www.sciencedirect.com/science/article/pii/0033589484900991>, 1984.
- Duplessy, J. C., Shackleton, N. J., Fairbanks, R. G., Labeyrie, L., Oppo, D. W., and Kallel, N.: Deepwater source variations during the last climatic cycle and their impact on the global deepwater circulation, *Paleoceanography*, 3, 343–360, <https://doi.org/10.1029/PA003i003p00343>, 1988.
- 465 Dutton, A. and Lambeck, K.: Ice Volume and Sea Level During the Last Interglacial, *Science*, 337, 216–219, <https://doi.org/10.1126/science.1205749>, <https://science.scienmag.org/content/337/6091/216>, 2012.
- Dutton, A., Carlson, A. E., Long, A. J., Milne, G. A., Clark, P. U., DeConto, R., Horton, B. P., Rahmstorf, S., and Raymo, M. E.: Sea-level rise due to polar ice-sheet mass loss during past warm periods, *Science*, 349, aaa4019, <https://doi.org/10.1126/science.aaa4019>, <http://science.scienmag.org/content/349/6244/aaa4019>, 2015.
- 470 Dyonisius, M. N., Petrenko, V. V., Smith, A. M., Hua, Q., Yang, B., Schmitt, J., Beck, J., Seth, B., Bock, M., Hmiel, B., Vimont, I., Menking, J. A., Shackleton, S. A., Baggenstos, D., Bauska, T. K., Rhodes, R. H., Sperlich, P., Beaudette, R., Harth, C., Kalk, M., Brook, E. J., Fischer, H., Severinghaus, J. P., and Weiss, R. F.: Old carbon reservoirs were not important in the deglacial methane budget, *Science*, 367, 907–910, <https://doi.org/10.1126/science.aax0504>, <https://science.scienmag.org/content/367/6480/907>, 2020.
- Egginton, S., Schmitt, J., Bereiter, B., Schneider, R., and Fischer, H.: CO<sub>2</sub> concentration and stable isotope ratios of three Antarctic ice cores covering the period from 149.4 - 1.5 kyr before 1950, PANGAEA, <https://doi.org/10.1594/PANGAEA.859181>, <https://doi.org/10.1594/PANGAEA.859181>, 2016.
- 480 Eide, M., Olsen, A., Ninnemann, U. S., and Johannessen, T.: A global ocean climatology of preindustrial and modern ocean  $\delta^{13}\text{C}$ , *Global Biogeochemical Cycles*, 31, 515–534, <https://doi.org/10.1002/2016GB005473>, <https://agupubs.onlinelibrary.wiley.com/doi/abs/10.1002/2016GB005473>, 2017.
- 485 Farquhar, G. D.: On the Nature of Carbon Isotope Discrimination in C4 Species, *Functional Plant Biology*, 10, 205–226, <https://doi.org/10.1071/PP9830205>, <https://www.publish.csiro.au/fp/PP9830205>, 1983.
- Farquhar, G. D., Ehleringer, J. R., and Hubick, K. T.: Carbon Isotope Discrimination and Photosynthesis, *Annual Review of Plant Physiology and Plant Molecular Biology*, 40, 503–537, <https://doi.org/10.1146/annurev.pp.40.060189.002443>, <https://www.annualreviews.org/doi/10.1146/annurev.pp.40.060189.002443>, 1989.
- 490 Flückiger, J., Monnin, E., Stauffer, B., Schwander, J., Stocker, T. F., Chappellaz, J., Raynaud, D., and Barnola, J.-M.: High-resolution Holocene N<sub>2</sub>O ice core record and its relationship with CH<sub>4</sub> and CO<sub>2</sub>, *Global Biogeochemical Cycles*, 16, 10–1–10–8, <https://doi.org/10.1029/2001GB001417>, <https://agupubs.onlinelibrary.wiley.com/doi/abs/10.1029/2001GB001417>, 2002.
- Freudenthal, T., Meggers, H., Henderiks, J., Kuhlmann, H., Moreno, A., and Wefer, G.: Upwelling intensity and filament activity off Morocco during the last 250,000 years, *Deep Sea Research Part II: Topical Studies in Oceanography*, 49, 3655–3674, [https://doi.org/10.1016/S0967-0645\(02\)00101-7](https://doi.org/10.1016/S0967-0645(02)00101-7), <http://www.sciencedirect.com/science/article/pii/S0967064502001017>, 2002.
- 495 Galaasen, E. V., Ninnemann, U. S., Irvali, N., Kleiven, H. F., Rosenthal, Y., Kissel, C., and Hodell, D. A.: Stable isotope ratios of C. wuellerstorfi from sediment core MD03-2664, Bjerknes Centre for Climate Research, <https://doi.org/10.1594/PANGAEA.830079>, <https://doi.pangaea.de/10.1594/PANGAEA.830079>, 2014a.

- Galaasen, E. V., Ninnemann, U. S., Ivali, N., Kleiven, H. K. F., Rosenthal, Y., Kissel, C., and Hodell, D. A.: Rapid Reductions in North  
500 Atlantic Deep Water During the Peak of the Last Interglacial Period, *Science*, 343, 1129–1132, <https://doi.org/10.1126/science.1248667>,  
<https://science.scienmag.org/content/343/6175/1129>, 2014b.
- Gebhardt, H., Sarnthein, M., Grootes, P. M., Kiefer, T., Kuehn, H., Schmieder, F., and Röhl, U.: Paleonutrient and productivity records from  
the subarctic North Pacific for Pleistocene glacial terminations I to V, *Paleoceanography*, 23, <https://doi.org/10.1029/2007PA001513>,  
<https://agupubs.onlinelibrary.wiley.com/doi/abs/10.1029/2007PA001513>, 2008.
- Govin, A., Braconnat, P., Capron, E., Cortijo, E., Duplessy, J.-C., Jansen, E., Labeyrie, L., Landais, A., Marti, O., Michel, E., Mosquet, E.,  
Risebrobakken, B., Swingedouw, D., and Waelbroeck, C.: Persistent influence of ice sheet melting on high northern latitude climate during  
the early Last Interglacial, *Climate of the Past*, 8, 483–507, <https://doi.org/https://doi.org/10.5194/cp-8-483-2012>, <https://www.clim-past.net/8/483/2012/>, 2012.
- Govin, A., Capron, E., Tzedakis, P. C., Verheyden, S., Ghaleb, B., Hillaire-Marcel, C., St-Onge, G., Stoner, J. S., Bassinot, F., Bazin, L.,  
510 Blunier, T., Combouieu-Nebout, N., El Ouahabi, A., Genty, D., Gersonde, R., Jimenez-Amat, P., Landais, A., Martrat, B., Masson-  
Delmotte, V., Parrenin, F., Seidenkrantz, M. S., Veres, D., Waelbroeck, C., and Zahn, R.: Sequence of events from the onset to the demise  
of the Last Interglacial: Evaluating strengths and limitations of chronologies used in climatic archives, *Quaternary Science Reviews*, 129,  
1–36, <https://doi.org/10.1016/j.quascirev.2015.09.018>, <http://www.sciencedirect.com/science/article/pii/S0277379115301165>, 2015.
- Hasenclever, J., Knorr, G., Rüpke, L. H., Köhler, P., Morgan, J., Garofalo, K., Barker, S., Lohmann, G., and Hall, I. R.: Sea  
515 level fall during glaciation stabilized atmospheric CO<sub>2</sub> by enhanced volcanic degassing, *Nature Communications*, 8, 15 867,  
<https://doi.org/10.1038/ncomms15867>, <http://www.nature.com/articles/ncomms15867>, 2017.
- Helmens, K. F., Salonen, J. S., Plikk, A., Engels, S., Välijanta, M., Kylander, M., Brendryen, J., and Renssen, H.: Major  
cooling intersecting peak Eemian Interglacial warmth in northern Europe, *Quaternary Science Reviews*, 122, 293–299,  
<https://doi.org/10.1016/j.quascirev.2015.05.018>, <http://www.sciencedirect.com/science/article/pii/S0277379115002231>, 2015.
- 520 Hmiel, B., Petrenko, V. V., Dyonisius, M. N., Buzert, C., Smith, A. M., Place, P. F., Harth, C., Beaudette, R., Hua, Q., Yang, B., Vimont,  
I., Michel, S. E., Severinghaus, J. P., Etheridge, D., Bromley, T., Schmitt, J., Faïn, X., Weiss, R. F., and Dlugokencky, E.: Preindustrial  
<sup>14</sup>CH<sub>4</sub> indicates greater anthropogenic fossil CH<sub>4</sub> emissions, *Nature*, 578, 409–412, <https://doi.org/10.1038/s41586-020-1991-8>, <http://www.nature.com/articles/s41586-020-1991-8>, 2020.
- Hodell, D., Charles, C., Curtis, J., Mortyn, P., Ninnemann, U., and Venz, K.: Data report: Oxygen isotope stratigraphy of ODP Leg 177 Sites  
525 1088, 1089, 1090, 1093, and 1094, in: Proc. Ocean Drill. Prog. Sci. Results, vol. 177, College Station TX (Ocean Drilling Program), 2003.
- Hodell, D. A. and Channell, J. E. T.: Mode transitions in Northern Hemisphere glaciation: co-evolution of millennial and orbital variability  
in Quaternary climate, *Climate of the Past*, 12, 1805–1828, <https://doi.org/https://doi.org/10.5194/cp-12-1805-2016>, <https://cp.copernicus.org/articles/12/1805/2016/>, 2016.
- Hodell, D. A., Charles, C. D., and Ninnemann, U. S.: Comparison of interglacial stages in the South Atlantic sector of the southern ocean for  
530 the past 450 kyr: implications for Marine Isotope Stage (MIS) 11, *Global and Planetary Change*, 24, 7–26, [https://doi.org/10.1016/S0921-8181\(99\)00069-7](https://doi.org/10.1016/S0921-8181(99)00069-7), <http://www.sciencedirect.com/science/article/pii/S0921818199000697>, 2000.
- Hodell, D. A., Charles, C. D., and Sierro, F. J.: Late Pleistocene evolution of the ocean's carbonate system, *Earth and Planetary Science Letters*, 192, 109–124, [https://doi.org/10.1016/S0012-821X\(01\)00430-7](https://doi.org/10.1016/S0012-821X(01)00430-7), <http://www.sciencedirect.com/science/article/pii/S0012821X01004307>, 2001.
- 535 Hodell, D. A., Channell, J. E. T., Curtis, J. H., Romero, O. E., and Röhl, U.: Oxygen and carbon isotopes of the benthic foraminifer  
Cibicides wuellerstorfi of IODP Site 303-U1308, In supplement to: Hodell, DA et al. (2008): Onset of 'Hudson Strait' Hein-

rich Events in the eastern North Atlantic at the end of the middle Pleistocene transition (~640 ka)? *Paleoceanography*, 23(4), PA4218, <https://doi.org/10.1029/2008PA001591>, <https://doi.org/10.1594/PANGAEA.831735>, <https://doi.pangaea.de/10.1594/PANGAEA.831735>, 2008.

- 540 Hoffman, J. S., Clark, P. U., Parnell, A. C., and He, F.: Regional and global sea-surface temperatures during the last interglaciation, *Science*, 355, 276–279, <https://doi.org/10.1126/science.aai8464>, <https://science.sciencemag.org/content/355/6322/276>, pMID:, 2017.
- Holbourn, A., Kuhnt, W., Schulz, M., and Erlenkeuser, H.: Impacts of orbital forcing and atmospheric carbon dioxide on Miocene ice-sheet expansion, *Nature*, 438, 483–487, <https://doi.org/10.1038/nature04123>, <https://www.nature.com/articles/nature04123>, 2005.
- Hoogakker, B. A. A., Rohling, E. J., Palmer, M. R., Tyrrell, T., and Rothwell, R. G.: Underlying causes for long-term global ocean  $\delta^{13}\text{C}$  fluctuations over the last 1.20 Myr, *Earth and Planetary Science Letters*, 248, 15–29, <https://doi.org/10.1016/j.epsl.2006.05.007>, <http://www.sciencedirect.com/science/article/pii/S0012821X06003402>, 2006.
- 545 Hüls, M.: Calculated sea surface temperature of sediment core M35003-4, *PANGAEA*, <https://doi.org/https://doi.org/10.1594/PANGAEA.55761>, <https://doi.pangaea.de/10.1594/PANGAEA.55761>, 1999.
- Huybers, P. and Langmuir, C.: Feedback between deglaciation, volcanism, and atmospheric CO<sub>2</sub>, *Earth and Planetary Science Letters*, 286, 479–491, <https://doi.org/10.1016/j.epsl.2009.07.014>, <http://www.sciencedirect.com/science/article/pii/S0012821X09004166>, 2009.
- IPCC: Climate Change 2013: The Physical Science Basis. Contribution of Working Group I to the Fifth Assessment Report of the Intergovernmental Panel on Climate Change, Tech. rep., Cambridge University Press, Cambridge, United Kingdom and New York, NY, USA, <https://www.ipcc.ch/report/ar5/wg1/>, 2013.
- Jansen, E., Raymo, M., and Blum, P.: Proc. ODP, Init. Repts, 154: College Station, TX (Ocean Drilling Program), <https://doi.org/10.2973/odp.proc.ir.162.1996>, 1996.
- 550 Jeltsch-Thömmes, A. and Joos, F.: The response to pulse-like perturbations in atmospheric carbon and carbon isotopes, *Climate of the Past Discussions*, pp. 1–36, <https://doi.org/https://doi.org/10.5194/cp-2019-107>, <https://www.clim-past-discuss.net/cp-2019-107/>, 2020.
- Jeltsch-Thömmes, A., Battaglia, G., Cartapanis, O., Jaccard, S. L., and Joos, F.: Low terrestrial carbon storage at the Last Glacial Maximum: constraints from multi-proxy data, *Climate of the Past*, 15, 849–879, <https://doi.org/z>, <https://www.clim-past.net/15/849/2019/>, 2019.
- 555 Jouzel, J., Masson-Delmotte, V., Cattani, O., Dreyfus, G., Falourd, S., Hoffmann, G., Minster, B., Nouet, J., Barnola, J. M., Chappellaz, J., Fischer, H., Gallet, J. C., Johnsen, S., Leuenberger, M., Louergue, L., Luethi, D., Oerter, H., Parrenin, F., Raisbeck, G., Raynaud, D., Schilt, A., Schwander, J., Selmo, E., Souchez, R., Spahni, R., Stauffer, B., Steffensen, J. P., Stenni, B., Stocker, T. F., Tison, J. L., Werner, M., and Wolff, E. W.: Orbital and Millennial Antarctic Climate Variability over the Past 800,000 Years, *Science*, 317, 793–796, <https://doi.org/10.1126/science.1141038>, <https://science.sciencemag.org/content/317/5839/793>, 2007.
- Jullien, E., Grousset, F. E., Hemming, S. R., Peck, V. L., Hall, I. R., Jeantet, C., and Billy, I.: Contrasting conditions preceding MIS3 and MIS2 Heinrich events, *Global and Planetary Change*, 54, 225–238, <https://doi.org/10.1016/j.gloplacha.2006.06.021>, <http://www.sciencedirect.com/science/article/pii/S0921818106001986>, 2006.
- Kawamura, K., Parrenin, F., Lisiecki, L., Uemura, R., Vimeux, F., Severinghaus, J. P., Hutterli, M. A., Nakazawa, T., Aoki, S., Jouzel, J., Raymo, M. E., Matsumoto, K., Nakata, H., Motoyama, H., Fujita, S., Goto-Azuma, K., Fujii, Y., and Watanabe, O.: Northern Hemisphere forcing of climatic cycles in Antarctica over the past 360,000 years, *Nature*, 448, 912–916, <https://doi.org/10.1038/nature06015>, <https://www.nature.com/articles/nature06015>, 2007.
- Keigwin, L. D. and Jones, G. A.: Glacial-Holocene stratigraphy, chronology, and paleoceanographic observations on some North Atlantic sediment drifts, *Deep Sea Research Part A. Oceanographic Research Papers*, 36, 845–867, [https://doi.org/10.1016/0198-0149\(89\)90032-0](https://doi.org/10.1016/0198-0149(89)90032-0), <http://www.sciencedirect.com/science/article/pii/0198014989900320>, 1989.

- 575 Keigwin, L. D. and Jones, G. A.: Western North Atlantic evidence for millennial-scale changes in ocean circulation and climate, *Journal of Geophysical Research: Oceans*, 99, 12 397–12 410, <https://doi.org/10.1029/94JC00525>, <http://agupubs.onlinelibrary.wiley.com/doi/abs/10.1029/94JC00525>, 1994.
- Keigwin, L. D. and Schlegel, M. A.: Ocean ventilation and sedimentation since the glacial maximum at 3 km in the western North Atlantic, *Geochemistry, Geophysics, Geosystems*, 3, 1–14, <https://doi.org/10.1029/2001GC000283>, <https://agupubs.onlinelibrary.wiley.com/doi/abs/10.1029/2001GC000283>, 2002.
- 580 Keigwin, L. D., Jones, G. A., Lehman, S. J., and Boyle, E. A.: Deglacial meltwater discharge, North Atlantic Deep Circulation, and abrupt climate change, *Journal of Geophysical Research: Oceans*, 96, 16 811–16 826, <https://doi.org/10.1029/91JC01624>, <https://agupubs.onlinelibrary.wiley.com/doi/abs/10.1029/91JC01624>, 1991.
- Keller, K. M., Lienert, S., Bozbiyik, A., Stocker, T. F., Churakova (Sidorova), O. V., Frank, D. C., Klesse, S., Koven, C. D., Leuenberger, M.,  
585 Riley, W. J., Saurer, M., Siegwolf, R., Weigt, R. B., and Joos, F.: 20th century changes in carbon isotopes and water-use efficiency: tree-ring-based evaluation of the CLM4.5 and LPX-Bern models, *Biogeosciences*, 14, 2641–2673, <https://doi.org/https://doi.org/10.5194/bg-14-2641-2017>, <https://www.biogeosciences.net/14/2641/2017/>, 2017.
- Key, R. M., Kozyr, A., Sabine, C. L., Lee, K., Wanninkhof, R., Bullister, J. L., Feely, R. A., Millero, F. J., Mordy, C., and Peng, T.-H.: A global ocean carbon climatology: Results from Global Data Analysis Project (GLODAP), *Global Biogeochemical Cycles*, 18,  
590 <https://doi.org/10.1029/2004GB002247>, <https://agupubs.onlinelibrary.wiley.com/doi/abs/10.1029/2004GB002247>, 2004.
- Köhler, P., Nehrbass-Ahles, C., Schmitt, J., Stocker, T. F., and Fischer, H.: Continuous record of the atmospheric greenhouse gas carbon dioxide (CO<sub>2</sub>), raw data, PANGAEA, <https://doi.org/10.1594/PANGAEA.871265>, <https://doi.pangaea.de/10.1594/PANGAEA.871265>, 2017.
- Kohn, M. J.: Carbon isotope compositions of terrestrial C3 plants as indicators of (paleo)ecology and (paleo)climate, *Proceedings of the National Academy of Sciences*, 107, 19 691–19 695, <https://doi.org/10.1073/pnas.1004933107>, <https://www.pnas.org/content/107/46/19691>,  
595 2010.
- Kopp, R. E., Simons, F. J., Mitrovica, J. X., Maloof, A. C., and Oppenheimer, M.: Probabilistic assessment of sea level during the last interglacial stage, *Nature*, 462, 863–867, <https://doi.org/10.1038/nature08686>, <http://www.nature.com/nature/journal/v462/n7275/full/nature08686.html?foxtrotcallback=true>, 2009.
- 600 Labeyrie, L., Vidal, L., Cortijo, E., Paterne, M., Arnold, M., Duplessy, J. C., Vautravers, M., Labracherie, M., Duprat, J., Turon, J. L., Grouset, F., and Van Weering, T.: Surface and Deep Hydrology of the Northern Atlantic Ocean during the past 150 000 Years, *Philosophical Transactions: Biological Sciences*, 348, 255–264, <https://www.jstor.org/stable/56044>, 1995.
- Labeyrie, L., Labracherie, M., Gorfti, N., Pichon, J. J., Vautravers, M., Arnold, M., Duplessy, J.-C., Paterne, M., Michel, E., Duprat, J., Caralp, M., and Turon, J.-L.: Hydrographic changes of the Southern Ocean (southeast Indian Sector) Over the last 230 kyr, *Paleoceanography*, 11, 57–76, <https://doi.org/10.1029/95PA02255>, <https://agupubs.onlinelibrary.wiley.com/doi/abs/10.1029/95PA02255>, 1996.
- 605 Labeyrie, L., Leclaire, H., Waelbroeck, C., Cortijo, E., Duplessy, J.-C., Vidal, L., Elliot, M., Coat, B. L., and Auffret, G.: Temporal Variability of the Surface and Deep Waters of the North West Atlantic Ocean at Orbital and Millenial Scales, in: *Mechanisms of Global Climate Change at Millennial Time Scales*, pp. 77–98, American Geophysical Union (AGU), <https://agupubs.onlinelibrary.wiley.com/doi/abs/10.1029/GM112p0077>, 1999.
- 610 Labeyrie, L. D., Leclaire, H., Waelbroeck, C., Cortijo, E., Duplessy, J.-C., Vidal, L., Elliot, M., and Le Coat, B.: Foraminiferal stable isotopes of sediment core CH69-K09, PANGAEA, <https://doi.org/https://doi.org/10.1594/PANGAEA.881464>, <https://doi.pangaea.de/10.1594/PANGAEA.881464>, 2017.

- Larrasoña, J. C., Roberts, A. P., and Rohling, E. J.: Dynamics of Green Sahara Periods and Their Role in Hominin Evolution, *PLOS ONE*, 8, e76514, <https://doi.org/10.1371/journal.pone.0076514>, <https://journals.plos.org/plosone/article?id=10.1371/journal.pone.0076514>, 2013.
- Laskar, J., Robutel, P., Joutel, F., Gastineau, M., Correia, A. C. M., and Levrard, B.: A long-term numerical solution for the insolation quantities of the Earth, *Astronomy & Astrophysics*, 428, 261–285, <https://doi.org/10.1051/0004-6361:20041335>, <http://www.aanda.org/10.1051/0004-6361:20041335>, 2004.
- Leavitt, S. W.: Systematics of stable-carbon isotopic differences between gymnosperm and angiosperm trees, *Plant Physiol. (Life Sci. Adv.)*, 11, 257–262, <https://ci.nii.ac.jp/naid/10028135088/>, 1992.
- Lebreiro, S. M., Voelker, A. H. L., Vizcaino, A., Abrantes, F. G., Alt-Epping, U., Jung, S., Thouveny, N., and Gràcia, E.: Sediment instability on the Portuguese continental margin under abrupt glacial climate changes (last 60kyr), *Quaternary Science Reviews*, 28, 3211–3223, <https://doi.org/10.1016/j.quascirev.2009.08.007>, <http://www.sciencedirect.com/science/article/pii/S027737910900273X>, 2009.
- Lee, M., Wei, K. C. J., and Chen, Y.-G.: High Resolution Oxygen Isotope Stratigraphy for the Last 150,000 Years in the Southern South China Sea: Core MD972151, *Terrestrial Atmospheric and Oceanic Sciences*, <https://doi.org/10.3319/tao.1999.10.1.239>(images), 1999.
- Lehman, S. J., Sachs, J. P., Crotwell, A. M., Keigwin, L. D., and Boyle, E. A.: Relation of subtropical Atlantic temperature, high-latitude ice rafting, deep water formation, and European climate 130,000–60,000 years ago, *Quaternary Science Reviews*, 21, 1917–1924, [https://doi.org/10.1016/S0277-3791\(02\)00078-1](https://doi.org/10.1016/S0277-3791(02)00078-1), <http://www.sciencedirect.com/science/article/pii/S0277379102000781>, 2002.
- Lisiecki, L. E. and Raymo, M. E.: A Pliocene-Pleistocene stack of 57 globally distributed benthic  $\delta^{18}\text{O}$  records, *Paleoceanography*, 20, PA1003, <https://doi.org/10.1029/2004PA001071>, <http://onlinelibrary.wiley.com/doi/10.1029/2004PA001071/abstract>, 2005.
- Lisiecki, L. E. and Stern, J. V.: Regional and global benthic  $\delta^{18}\text{O}$  stacks for the last glacial cycle, *Paleoceanography*, 31, 2016PA003002, <https://doi.org/10.1002/2016PA003002>, <http://onlinelibrary.wiley.com/doi/10.1002/2016PA003002/abstract>, 2016.
- Lototskaya, A. and Ganssen, G. M.: The structure of Termination II (penultimate deglaciation and Eemian) in the North Atlantic, *Quaternary Science Reviews*, 18, 1641–1654, [https://doi.org/10.1016/S0277-3791\(99\)00011-6](https://doi.org/10.1016/S0277-3791(99)00011-6), <http://www.sciencedirect.com/science/article/pii/S0277379199000116>, 1999.
- Lüthi, D., Le Floch, M., Bereiter, B., Blunier, T., Barnola, J.-M., Siegenthaler, U., Raynaud, D., Jouzel, J., Fischer, H., Kawamura, K., and Stocker, T. F.: High-resolution carbon dioxide concentration record 650,000–800,000 years before present, *Nature*, 453, 379–382, <https://doi.org/10.1038/nature06949>, <https://www.nature.com/articles/nature06949>, 2008.
- Lyle, M., Mix, A., and Pisias, N.: Patterns of  $\text{CaCO}_3$  deposition in the eastern tropical Pacific Ocean for the last 150 Kyr: Evidence for a south-east Pacific depositional spike during marine isotope stage (MIS) 2, *Paleoceanography*, 17, 3–1, <https://doi.org/10.1029/2000PA000538>, 2002.
- Lynch-Stieglitz, J., Stocker, T. F., Broecker, W. S., and Fairbanks, R. G.: The influence of air-sea exchange on the isotopic composition of oceanic carbon: Observations and modeling, *Global Biogeochemical Cycles*, 9, 653–665, <https://doi.org/10.1029/95GB02574>, <https://agupubs.onlinelibrary.wiley.com/doi/abs/10.1029/95GB02574>, 1995.
- Lynch-Stieglitz, J., Curry, W. B., Oppo, D. W., Ninneman, U. S., Charles, C. D., and Munson, J.: Meridional overturning circulation in the South Atlantic at the last glacial maximum, *Geochemistry, Geophysics, Geosystems*, 7, <https://doi.org/10.1029/2005GC001226>, <https://agupubs.onlinelibrary.wiley.com/doi/abs/10.1029/2005GC001226>, 2006.
- Mackensen, A. and Bickert, T.: Stable Carbon Isotopes in Benthic Foraminifera: Proxies for Deep and Bottom Water Circulation and New Production, in: *Use of Proxies in Paleoceanography: Examples from the South Atlantic*, edited by Fischer, G. and Wefer, G., pp. 229–254, Springer, Berlin, Heidelberg, [https://doi.org/10.1007/978-3-642-58646-0\\_9](https://doi.org/10.1007/978-3-642-58646-0_9), 1999.

- Mackensen, A., Rudolph, M., and Kuhn, G.: Late Pleistocene deep-water circulation in the subantarctic eastern Atlantic, Global  
650 and Planetary Change, 30, 197–229, [https://doi.org/10.1016/S0921-8181\(01\)00102-3](https://doi.org/10.1016/S0921-8181(01)00102-3), <http://www.sciencedirect.com/science/article/pii/S0921818101001023>, 2001.
- Marcott, S. A., Shakun, J. D., Clark, P. U., and Mix, A. C.: A Reconstruction of Regional and Global Temperature for the Past 11,300 Years, Science, 339, 1198–1201, <https://doi.org/10.1126/science.1228026>, <https://science.sciencemag.org/content/339/6124/1198>, 2013.
- Martrat, B., Grimalt, J. O., Shackleton, N. J., de Abreu, L., Hutterli, M. A., and Stocker, T. F.: Sea surface temperature estimation for the  
655 Iberian Margin, Supplement to: Martrat, B et al. (2007): Four climate cycles of recurring deep and surface water destabilizations on the Iberian Margin. Science, 317(5837), 502–507, <https://doi.org/10.1126/science.1139994>, <https://doi.org/10.1594/PANGAEA.771894>, <https://doi.pangaea.de/10.1594/PANGAEA.771894>, 2007a.
- Martrat, B., Grimalt, J. O., Shackleton, N. J., de Abreu, L., Hutterli, M. A., and Stocker, T. F.: (Table S2) Sea surface temperature estimation for ODP Hole 161-977A, PANGAEA, <https://doi.org/10.1594/PANGAEA.771890>, <https://doi.pangaea.de/10.1594/PANGAEA.771890>,  
660 2007b.
- Masson-Delmotte, V., Stenni, B., Pol, K., Braconnot, P., Cattani, O., Falourd, S., Kageyama, M., Jouzel, J., Landais, A., Minster, B., Barnola,  
J. M., Chappellaz, J., Krinner, G., Johnsen, S., Röhlisberger, R., Hansen, J., Mikolajewicz, U., and Otto-Bliesner, B.: EPICA Dome C record of glacial and interglacial intensities, Quaternary Science Reviews, 29, 113–128, <https://doi.org/10.1016/j.quascirev.2009.09.030>,  
<http://www.sciencedirect.com/science/article/pii/S0277379109003369>, 2010.
- 665 Masson-Delmotte, V., Schulz, M., Abe-Ouchi, A., Beer, J., Ganopolski, J., González Rouco, J. F., Jansen, E., Lambeck, K., Luterbacher, J., Naish, T., Osborn, T., Otto-Bliesner, B., Quinn, T., Ramesh, R., Rojas, M., Shao, X., and Timmermann, A.: Information from paleoclimate archives, in: Climate change 2013: The physical science basis. Contribution of working group I to the fifth assessment report of the intergovernmental panel on climate change, edited by Stocker, T. F., Qin, D., Plattner, G.-K., Tignor, M., Allen, S. K., Doschung, J., Nauels, A., Xia, Y., Bex, V., and Midgley, P. M., pp. 383–464, Cambridge University Press, Cambridge, UK,  
670 <https://doi.org/10.1017/CBO9781107415324.013>, 2013.
- McCorkle, D. and Holder, A.: Calibration Studies of Benthic Foraminiferal Isotopic Composition: Results from the Southeast Pacific, AGU Fall Meeting Abstracts, 2001.
- McIntyre, K., Ravelo, A. C., and Delaney, M. L.: North Atlantic Intermediate Waters in the Late Pliocene to Early Pleistocene, Paleoceanography, 14, 324–335, <https://doi.org/10.1029/1998PA900005>, <https://agupubs.onlinelibrary.wiley.com/doi/abs/10.1029/1998PA900005>,  
675 1999.
- McKay, N. P., Overpeck, J. T., and Otto-Bliesner, B. L.: The role of ocean thermal expansion in Last Interglacial sea level rise, Geophysical Research Letters, 38, <https://doi.org/10.1029/2011GL048280>, <https://agupubs.onlinelibrary.wiley.com/doi/abs/10.1029/2011GL048280>, 2011.
- McManus, J. F., Oppo, D. W., and Cullen, J. L.: A 0.5-Million-Year Record of Millennial-Scale Climate Variability in the North Atlantic,  
680 Science, 283, 971–975, <https://doi.org/10.1126/science.283.5404.971>, <https://science.sciencemag.org/content/283/5404/971>, 1999.
- Members, C. P.: Stable isotopes measured on foraminifera from the 120 kyr time slice reconstruction in sediment core RC12-339, PANGAEA, <https://doi.org/https://doi.org/10.1594/PANGAEA.358927>, <https://doi.pangaea.de/10.1594/PANGAEA.358927>, 2006.
- Menviel, L. and Joos, F.: Toward explaining the Holocene carbon dioxide and carbon isotope records: Results from transient ocean carbon cycle-climate simulations, Paleoceanography, 27, <https://doi.org/10.1029/2011PA002224>, <https://agupubs.onlinelibrary.wiley.com/doi/abs/10.1029/2011PA002224>, 2012.

- Menviel, L., Mouchet, A., J. Meissner, K., Joos, F., and H. England, M.: Impact of oceanic circulation changes on atmospheric  $\delta^{13}\text{CO}_2$ , *Global Biogeochemical Cycles*, 29, 1944–1961, <https://doi.org/10.1002/2015GB005207>, 2015.
- Menviel, L., Yu, J., Joos, F., Mouchet, A., Meissner, K. J., and England, M. H.: Poorly ventilated deep ocean at the Last Glacial Maximum inferred from carbon isotopes: A data-model comparison study, *Paleoceanography*, 32, 2–17, <https://doi.org/10.1002/2016PA003024>, 2017.
- 690 Men viel, L., Capron, E., Govin, A., Dutton, A., Tarasov, L., Abe-Ouchi, A., Drysdale, R. N., Gibbard, P. L., Gregoire, L., He, F., Ivanovic, R. F., Kageyama, M., Kawamura, K., Landais, A., Otto-Bliesner, B. L., Oyabu, I., Tzedakis, P. C., Wolff, E., and Zhang, X.: The penultimate deglaciation: protocol for Paleoclimate Modelling Intercomparison Project (PMIP) phase 4 transient numerical simulations between 140 and 127 ka, version 1.0, *Geoscientific Model Development*, 12, 3649–3685, [https://doi.org/https://doi.org/10.5194/gmd-12-3649-2019](https://doi.org/10.5194/gmd-12-3649-2019), 2019, <https://www.geosci-model-dev.net/12/3649/2019/gmd-12-3649-2019.html>, 2019.
- Millo, C., Sarnthein, M., Voelker, A., and Erlenkeuser, H.: Variability of the Denmark Strait Overflow during the Last Glacial Maximum, *Boreas*, 35, 50–60, <https://doi.org/10.1080/03009480500359244>, 2006.
- Mix, A. C. and Fairbanks, R. G.: North Atlantic surface-ocean control of Pleistocene deep-ocean circulation, *Earth and Planetary Science Letters*, 73, 231–243, [https://doi.org/10.1016/0012-821X\(85\)90072-X](https://doi.org/10.1016/0012-821X(85)90072-X), <http://www.sciencedirect.com/science/article/pii/0012821X8590072X>, 1985.
- 700 Mix, A. C., Pisias, N. G., Zahn, R., Rugh, W., Lopez, C., and Nelson, K.: Carbon 13 in Pacific Deep and Intermediate Waters, 0–370 ka: Implications for Ocean Circulation and Pleistocene CO<sub>2</sub>, *Paleoceanography*, 6, 205–226, <https://doi.org/10.1029/90PA02303>, <https://agupubs.onlinelibrary.wiley.com/doi/abs/10.1029/90PA02303>, 1991.
- Mokeddem, Z., McManus, J. F., and Oppo, D. W.: Oceanographic dynamics and the end of the last interglacial in the subpolar North Atlantic, *Proceedings of the National Academy of Sciences*, 111, 11 263–11 268, <https://doi.org/10.1073/pnas.1322103111>, <https://www.pnas.org/content/111/31/11263>, 2014.
- 710 Montero-Serrano, J.-C., Bout-Roumazeilles, V., Carlson, A. E., Tribouillard, N., Bory, A., Meunier, G., Sionneau, T., Flower, B. P., Martinez, P., Billy, I., and Riboulleau, A.: Contrasting rainfall patterns over North America during the Holocene and Last Interglacial as recorded by sediments of the northern Gulf of Mexico, *Geophysical Research Letters*, 38, <https://doi.org/10.1029/2011GL048194>, <https://agupubs.onlinelibrary.wiley.com/doi/abs/10.1029/2011GL048194>, 2011.
- Muhs, D. R., Ager, T. A., and Begét, J. E.: Vegetation and paleoclimate of the last interglacial period, central Alaska, *Quaternary Science Reviews*, 20, 41–61, [https://doi.org/10.1016/S0277-3791\(00\)00132-3](https://doi.org/10.1016/S0277-3791(00)00132-3), <http://www.sciencedirect.com/science/article/pii/S0277379100001323>, 2001.
- Mulitza, S., Prange, M., Stuut, J.-B., Zabel, M., Dobeneck, T. v., Itambi, A. C., Nizou, J., Schulz, M., and Wefer, G.: Sahel megadroughts triggered by glacial slowdowns of Atlantic meridional overturning, *Paleoceanography*, 23, <https://doi.org/10.1029/2008PA001637>, <https://agupubs.onlinelibrary.wiley.com/doi/abs/10.1029/2008PA001637>, 2008.
- 720 Novák, M., Buzek, F., and Adamová, M.: Vertical trends in  $\delta^{13}\text{C}$ ,  $\delta^{15}\text{N}$  and  $\delta^{34}\text{S}$  ratios in bulk Sphagnum peat, *Soil Biology and Biochemistry*, 31, 1343–1346, Martin, 1999.
- of PAGES, P. I. W. G.: Interglacials of the last 800,000 years, *Reviews of Geophysics*, 54, 162–219, <https://doi.org/10.1002/2015RG000482>, 2016.
- Oliver, K. I. C., Hoogakker, B. A. A., Crowhurst, S., Henderson, G. M., Rickaby, R. E. M., Edwards, N. R., and Elderfield, H.: A synthesis of marine sediment core  $\delta^{13}\text{C}$  data over the last 150 000 years, *Climate of the Past*, 5, 2497–2554, <https://doi.org/10.5194/cpd-5-2497-2009>, <https://eprints.soton.ac.uk/164615/>, 2010.

- Oppo, D. W. and Fairbanks, R. G.: Variability in the deep and intermediate water circulation of the Atlantic Ocean during the  
725 past 25,000 years: Northern Hemisphere modulation of the Southern Ocean, *Earth and Planetary Science Letters*, 86, 1–15,  
[https://doi.org/10.1016/0012-821X\(87\)90183-X](https://doi.org/10.1016/0012-821X(87)90183-X), <http://www.sciencedirect.com/science/article/pii/0012821X8790183X>, 1987.
- Oppo, D. W. and Horowitz, M.: Glacial deep water geometry: South Atlantic benthic foraminiferal Cd/Ca and  $\delta^{13}\text{C}$  evidence, *Paleoceanography*, 15, 147–160, <https://doi.org/10.1029/1999PA000436>, <https://agupubs.onlinelibrary.wiley.com/doi/abs/10.1029/1999PA000436>, 2000.
- 730 Oppo, D. W. and Lehman, S. J.: Suborbital timescale variability of North Atlantic Deep Water during the past 200,000 years, *Paleoceanography*, 10, 901–910, <https://doi.org/10.1029/95PA02089>, <https://agupubs.onlinelibrary.wiley.com/doi/abs/10.1029/95PA02089>, 1995.
- Oppo, D. W., McManus, J. F., and Cullen, J. L.: Abrupt Climate Events 500,000 to 340,000 Years Ago: Evidence from Subpolar North Atlantic Sediments, *Science*, 279, 1335–1338, <https://doi.org/10.1126/science.279.5355.1335>, <https://science.scienmag.org/content/279/5355/1335>, 1998.
- 735 Oppo, D. W., McManus, J. F., and Cullen, J. L.: Evolution and demise of the Last Interglacial warmth in the subpolar North Atlantic, *Quaternary Science Reviews*, 25, 3268–3277, <https://doi.org/10.1016/j.quascirev.2006.07.006>, <http://www.sciencedirect.com/science/article/pii/S0277379106002319>, 2006.
- Otto-Bliesner, B., Brady, E., Zhao, A., Brierley, C., Axford, Y., Capron, E., Govin, A., Hoffman, J., Isaacs, E., Kageyama, M., Scussolini, P.,  
740 Tzedakis, P. C., Williams, C., Wolff, E., Abe-Ouchi, A., Braconnot, P., Ramos Buarque, S., Cao, J., de Vernal, A., Guarino, M. V., Guo, C., LeGrande, A. N., Lohmann, G., Meissner, K., Menziel, L., Nisancioglu, K., O’ishi, R., Salas Y Melia, D., Shi, X., Sicard, M., Sime, L., Tomas, R., Volodin, E., Yeung, N., Zhang, Q., Zhang, Z., and Zheng, W.: Large-scale features of Last Interglacial climate: Results from evaluating the lig127k simulations for CMIP6-PMIP4, *Climate of the Past Discussions*, <https://doi.org/https://doi.org/10.5194/cp-2019-174>, <https://www.clim-past-discuss.net/cp-2019-174/>, 2020.
- Pahnke, K. and Zahn, R.: Southern Hemisphere water mass conversion linked with North Atlantic climate variability, *Science (New York, N.Y.)*, 307, 1741–1746, <https://doi.org/10.1126/science.1102163>, 2005.
- 745 Peterson, C. D., Lisiecki, L. E., and Stern, J. V.: Deglacial whole-ocean  $\delta^{13}\text{C}$  change estimated from 480 benthic foraminiferal records, *Paleoceanography*, 29, 549–563, <https://doi.org/10.1002/2013PA002552>, <https://agupubs.onlinelibrary.wiley.com/doi/abs/10.1002/2013PA002552>, 2014.
- Petit, J. R., Jouzel, J., Raynaud, D., Barkov, N. I., Barnola, J.-M., Basile, I., Bender, M., Chappellaz, J., Davis, M., Delaygue, G., Delmotte, M., Kotlyakov, V. M., Legrand, M., Lipenkov, V. Y., Lorius, C., Pépin, L., Ritz, C., Saltzman, E., and Stievenard, M.: Climate and atmospheric history of the past 420,000 years from the Vostok ice core, Antarctica, *Nature*, 399, 429–436, <https://doi.org/10.1038/20859>, <https://www.nature.com/articles/20859>, 1999.
- Pisias, N. G. and Mix, A. C.: Spatial and temporal oceanographic variability of the eastern equatorial Pacific during the Late Pleistocene: Evidence from radiolaria microfossils, *Paleoceanography*, 12, 381–393, <https://doi.org/10.1029/97PA00583>, <https://agupubs.onlinelibrary.wiley.com/doi/abs/10.1029/97PA00583>, 1997.
- Rau, A. J., Rogers, J., Lutjeharms, J. R. E., Giraudeau, J., Lee-Thorp, J. A., Chen, M. T., and Waelbroeck, C.: A 450-kyr record of hydrological conditions on the western Agulhas Bank Slope, south of Africa, *Marine Geology*, 180, 183–201, [https://doi.org/10.1016/S0025-3227\(01\)00213-4](https://doi.org/10.1016/S0025-3227(01)00213-4), <http://www.sciencedirect.com/science/article/pii/S0025322701002134>, 2002.
- 750 Raymo, M. E., Oppo, D. W., and Curry, W.: The Mid-Pleistocene climate transition: A deep sea carbon isotopic perspective, *Paleoceanography*, 12, 546–559, <https://doi.org/10.1029/97PA01019>, <https://agupubs.onlinelibrary.wiley.com/doi/abs/10.1029/97PA01019>, 1997.

- Raymo, M. E., Oppo, D. W., Flower, B. P., Hodell, D. A., McManus, J. F., Venz, K. A., Kleiven, K. F., and McIntyre, K.: Stability of North Atlantic water masses in face of pronounced climate variability during the Pleistocene, *Paleoceanography*, 19, https://doi.org/10.1029/2003PA000921, https://agupubs.onlinelibrary.wiley.com/doi/abs/10.1029/2003PA000921, 2004.
- Reyes, A. V., Froese, D. G., and Jensen, B. J. L.: Permafrost response to last interglacial warming: field evidence from non-glaciated Yukon and Alaska, *Quaternary Science Reviews*, 29, 3256–3274, https://doi.org/10.1016/j.quascirev.2010.07.013, http://www.sciencedirect.com/science/article/pii/S0277379110002647, 2010.
- Roth, R. and Joos, F.: Model limits on the role of volcanic carbon emissions in regulating glacial–interglacial CO<sub>2</sub> variations, *Earth and Planetary Science Letters*, 329–330, 141–149, https://doi.org/10.1016/j.epsl.2012.02.019, http://www.sciencedirect.com/science/article/pii/S0012821X12001094, 2012.
- Rowe, P. J., Wickens, L. B., Sahy, D., Marca, A. D., Peckover, E., Noble, S., Özkul, M., Baykara, M. O., Millar, I. L., and Andrews, J. E.: Multi-proxy speleothem record of climate instability during the early last interglacial in southern Turkey, *Palaeogeography, Palaeoclimatology, Palaeoecology*, p. 109422, https://doi.org/10.1016/j.palaeo.2019.109422, http://www.sciencedirect.com/science/article/pii/S0031018219302214, 2019.
- Ruddiman, W. F. and Members, C. P.: Stable isotope data of the 120 k time slice, PANGAEA, https://doi.org/10.1594/PANGAEA.51932, https://doi.pangaea.de/10.1594/PANGAEA.51932, 1982.
- Russon, T., Elliot, M., Kissel, C., Cabioch, G., Deckker, P. D., and Corrège, T.: Middle-late Pleistocene deep water circulation in the southwest subtropical Pacific, *Paleoceanography*, 24, https://doi.org/10.1029/2009PA001755, https://agupubs.onlinelibrary.wiley.com/doi/abs/10.1029/2009PA001755, 2009.
- Samson, C. R., Sikes, E. L., and Howard, W. R.: Deglacial paleoceanographic history of the Bay of Plenty, New Zealand, *Paleoceanography*, 20, https://doi.org/10.1029/2004PA001088, https://agupubs.onlinelibrary.wiley.com/doi/abs/10.1029/2004PA001088, 2005.
- Sarnthein, M.: Age model of sediment core GIK16772-1, PANGAEA, https://doi.org/https://doi.org/10.1594/PANGAEA.134239, https://doi.pangaea.de/10.1594/PANGAEA.134239, 2003.
- Sarnthein, M., Winn, K., Jung, S. J. A., Duplessy, J.-C., Labeyrie, L., Erlenkeuser, H., and Ganssen, G.: Changes in East Atlantic Deepwater Circulation over the last 30,000 years: Eight time slice reconstructions, *Paleoceanography*, 9, 209–267, https://doi.org/10.1029/93PA03301, https://agupubs.onlinelibrary.wiley.com/doi/abs/10.1029/93PA03301, 1994.
- Saunois, M., Stavert, A. R., Poulter, B., Bousquet, P., Canadell, J. G., Jackson, R. B., Raymond, P. A., Dlugokencky, E. J., Houweling, S., Patra, P. K., Ciais, P., Arora, V. K., Bastviken, D., Bergamaschi, P., Blake, D. R., Brailsford, G., Bruhwiler, L., Carlson, K. M., Carroll, M., Castaldi, S., Chandra, N., Crevoisier, C., Crill, P. M., Covey, K., Curry, C. L., Etiope, G., Frankenberg, C., Gedney, N., Hegglin, M. I., Höglund-Isaksson, L., Hugelius, G., Ishizawa, M., Ito, A., Janssens-Maenhout, G., Jensen, K. M., Joos, F., Kleinen, T., Krummel, P. B., Langenfelds, R. L., Laruelle, G. G., Liu, L., Machida, T., Maksyutov, S., McDonald, K. C., McNorton, J., Miller, P. A., Melton, J. R., Morino, I., Müller, J., Murguia-Flores, F., Naik, V., Niwa, Y., Noce, S., O'Doherty, S., Parker, R. J., Peng, C., Peng, S., Peters, G. P., Prigent, C., Prinn, R., Ramonet, M., Regnier, P., Riley, W. J., Rosentreter, J. A., Segers, A., Simpson, I. J., Shi, H., Smith, S. J., Steele, L. P., Thornton, B. F., Tian, H., Tohjima, Y., Tubiello, F. N., Tsuruta, A., Viovy, N., Voulgarakis, A., Weber, T. S., van Weele, M., van der Werf, G. R., Weiss, R. F., Worthy, D., Wunch, D., Yin, Y., Yoshida, Y., Zhang, W., Zhang, Z., Zhao, Y., Zheng, B., Zhu, Q., Zhu, Q., and Zhuang, Q.: The Global Methane Budget 2000–2017, *Earth System Science Data*, 12, 1561–1623, https://doi.org/https://doi.org/10.5194/essd-12-1561-2020, https://essd.copernicus.org/articles/12/1561/2020/, 2020.

- Schmiedl, G. and Mackensen, A.: Late Quaternary paleoproductivity and deep water circulation in the eastern South Atlantic Ocean: Evidence from benthic foraminifera, *Palaeogeography, Palaeoclimatology, Palaeoecology*, 130, 43–80, [https://doi.org/10.1016/S0031-0182\(96\)00137-X](https://doi.org/10.1016/S0031-0182(96)00137-X), <http://www.sciencedirect.com/science/article/pii/S003101829600137X>, 1997.
- 800 Schmiedl, G. and Mackensen, A.: Multispecies stable isotopes of benthic foraminifers reveal past changes of organic matter decomposition and deepwater oxygenation in the Arabian Sea, *Paleoceanography*, 21, <https://doi.org/10.1029/2006PA001284>, <https://agupubs.onlinelibrary.wiley.com/doi/abs/10.1029/2006PA001284>, 2006.
- Schmittner, A., Gruber, N., Mix, A. C., Key, R. M., Tagliabue, A., and Westberry, T. K.: Biology and air-sea gas exchange controls on the distribution of carbon isotope ratios ( $\delta^{13}\text{C}$ ) in the ocean, *Biogeosciences*, 10, 5793–5816, <https://doi.org/10.5194/bg-10-5793-2013>, <https://www.biogeosciences.net/10/5793/2013/>, 2013.
- 805 Schneider, R., Schmitt, J., Köhler, P., Joos, F., and Fischer, H.: A reconstruction of atmospheric carbon dioxide and its stable carbon isotopic composition from the penultimate glacial maximum to the last glacial inception, *Climate of the Past*, 9, 2507–2523, <https://doi.org/10.5194/cp-9-2507-2013>, <http://www.clim-past.net/9/2507/2013/>, 2013.
- Schönenfeld, J., Zahn, R., and de Abreu, L.: Surface and deep water response to rapid climate changes at the Western Iberian Margin, *Global and Planetary Change*, 36, 237–264, [https://doi.org/10.1016/S0921-8181\(02\)00197-2](https://doi.org/10.1016/S0921-8181(02)00197-2), <http://www.sciencedirect.com/science/article/pii/S0921818102001972>, 2003.
- 810 Schubert, B. A. and Jahren, A. H.: The effect of atmospheric CO<sub>2</sub> concentration on carbon isotope fractionation in C3 land plants, *Geochimica et Cosmochimica Acta*, 96, 29–43, <https://doi.org/10.1016/j.gca.2012.08.003>, <http://www.sciencedirect.com/science/article/pii/S0016703712004504>, 2012.
- 815 Schuur, E. a. G., McGuire, A. D., Schädel, C., Grosse, G., Harden, J. W., Hayes, D. J., Hugelius, G., Koven, C. D., Kuhry, P., Lawrence, D. M., Natali, S. M., Olefeldt, D., Romanovsky, V. E., Schaefer, K., Turetsky, M. R., Treat, C. C., and Vonk, J. E.: Climate change and the permafrost carbon feedback, *Nature*, 520, 171–179, <https://doi.org/10.1038/nature14338>, <https://www.nature.com/articles/nature14338>, 2015.
- Shackleton, N., Hall, M., and Pate, D.: Pliocene stable isotope stratigraphy of ODP Site 846, Tech. Rep. 138, International Ocean Discovery Program, 1995.
- 820 Shackleton, N. J.: The last interglacial in the marine and terrestrial records, *Proceedings of the Royal Society of London. Series B. Biological Sciences*, 174, 135–154, <https://doi.org/10.1098/rspb.1969.0085>, <https://royalsocietypublishing.org/doi/10.1098/rspb.1969.0085>, 1969.
- Shackleton, N. J.: Stable carbon and oxygen isotope ratios of benthic and planktic foraminifera from the Atlantic Ocean, Supplement to: Shackleton, NJ (1977): Carbon-13 in Uvigerina: Tropical rain forest history and the equatorial Pacific carbonate dissolution cycle. In: Andersen, N R & Malahoff, A (eds.), *The Fate of Fossil Fuel in the Oceans*. New York (Plenum), 401–427, <https://doi.org/https://doi.org/10.1594/PANGAEA.692091>, <https://doi.pangaea.de/10.1594/PANGAEA.692091>, 1977.
- 825 Shackleton, N. J. and Hall, M. A.: Stable isotope record of DSDP Hole 81-552A in the northeastern Atlantic Ocean, Supplement to: Shackleton, NJ; Hall, MA (1984): Oxygen and carbon isotope stratigraphy of Deep Sea Drilling Project Hole 552A: Plio-Pleistocene glacial history. In: Roberts, DG; Schnittker, D; et al. (eds.), *Initial Reports of the Deep Sea Drilling Project*, Washington (U.S. Govt. Printing Office), 81, 599–609, <https://doi.org/10.2973/dsdp.proc.81.116.1984>, <https://doi.org/https://doi.org/10.1594/PANGAEA.698993>, <https://doi.pangaea.de/10.1594/PANGAEA.698993>, 1984.
- Shackleton, N. J., Berger, A., and Peltier, W. R.: An alternative astronomical calibration of the lower Pleistocene timescale based on ODP Site 677, *Earth and Environmental Science Transactions of The Royal Society of Edinburgh*, 81, 251–261, <https://doi.org/10.1017/S0263593300020782>, <https://doi.org/10.1017/S0263593300020782>

- 835 //www.cambridge.org/core/journals/earth-and-environmental-science-transactions-of-royal-society-of-edinburgh/article/an-alternative-astronomical-calibration-of-the-lower-pleistocene-timescale-based-on-odp-site-677/D02E93BFBF418256AD00642C8A98277C, 1990.
- Shackleton, N. J., Hall, M. A., and Vincent, E.: Phase relationships between millennial-scale events 64,000–24,000 years ago, Paleoceanography, 15, 565–569, <https://doi.org/10.1029/2000PA000513>, <https://agupubs.onlinelibrary.wiley.com/doi/abs/10.1029/2000PA000513>, 840 2000.
- Shackleton, S., Baggenstos, D., Menking, J. A., Dyonisius, M. N., Bereiter, B., Bauska, T. K., Rhodes, R. H., Brook, E. J., Petrenko, V. V., McConnell, J. R., Kellerhals, T., Häberli, M., Schmitt, J., Fischer, H., and Severinghaus, J. P.: Global ocean heat content in the Last Inter-glacial, Nature Geoscience, 13, 77–81, <https://doi.org/10.1038/s41561-019-0498-0>, <https://www.nature.com/articles/s41561-019-0498-0>, 2020.
- 845 Sikes, E. L., Howard, W. R., Samson, C. R., Mahan, T. S., Robertson, L. G., and Volkman, J. K.: Southern Ocean seasonal temperature and Subtropical Front movement on the South Tasman Rise in the late Quaternary, Paleoceanography, 24, <https://doi.org/10.1029/2008PA001659>, <https://agupubs.onlinelibrary.wiley.com/doi/abs/10.1029/2008PA001659>, 2009.
- Sirocko, F., Garbe-Schönberg, D., and Devey, C.: Processes controlling trace element geochemistry of Arabian Sea sediments during the last 25,000 years, Global and Planetary Change, 26, 217–303, [https://doi.org/10.1016/S0921-8181\(00\)00046-1](https://doi.org/10.1016/S0921-8181(00)00046-1), <http://www.sciencedirect.com/science/article/pii/S0921818100000461>, 2000.
- 850 Skinner, L. C. and Shackleton, N. J.: Rapid transient changes in northeast Atlantic deep water ventilation age across Termination I, Paleoceanography, 19, <https://doi.org/10.1029/2003PA000983>, <https://agupubs.onlinelibrary.wiley.com/doi/abs/10.1029/2003PA000983>, 2004.
- Skinner, L. C. and Shackleton, N. J.: An Atlantic lead over Pacific deep-water change across Termination I: implications for the application of the marine isotope stage stratigraphy., Quaternary Science Reviews, 24, 571–580, [https://doi.org/Skinner, L. C. and Shackleton, N. J. \(2005\) An Atlantic lead over Pacific deep-water change across Termination I: implications for the application of the marine isotope stage stratigraphy. Quaternary Science Reviews, 24. pp. 571-580. DOI https://doi.org/10.1016/j.quascirev.2004.11.008, http://eprints.esc.cam.ac.uk/1830/](https://doi.org/Skinner, L. C. and Shackleton, N. J. (2005) An Atlantic lead over Pacific deep-water change across Termination I: implications for the application of the marine isotope stage stratigraphy. Quaternary Science Reviews, 24. pp. 571-580. DOI https://doi.org/10.1016/j.quascirev.2004.11.008, http://eprints.esc.cam.ac.uk/1830/), 2005.
- 855 Skinner, L. C., Shackleton, N. J., and Elderfield, H.: Millennial-scale variability of deep-water temperature and  $\delta^{18}\text{O}_{\text{dw}}$  indicating deep-water source variations in the Northeast Atlantic, 0–34 cal. ka BP, Geochemistry, Geophysics, Geosystems, 4, <https://doi.org/10.1029/2003GC000585>, <https://agupubs.onlinelibrary.wiley.com/doi/abs/10.1029/2003GC000585>, 2003.
- Sowers, T., Bender, M., Labeyrie, L., Martinson, D., Jouzel, J., Raynaud, D., Pichon, J. J., and Korotkevich, Y. S.: A 135,000-year Vostok-Specmap Common temporal framework, Paleoceanography, 8, 737–766, <https://doi.org/10.1029/93PA02328>, <https://agupubs.onlinelibrary.wiley.com/doi/abs/10.1029/93PA02328>, 1993.
- Spahni, R., Chappellaz, J., Stocker, T. F., Loulergue, L., Hausmann, G., Kawamura, K., Flückiger, J., Schwander, J., Raynaud, D., Masson-Delmotte, V., and Jouzel, J.: Atmospheric Methane and Nitrous Oxide of the Late Pleistocene from Antarctic Ice Cores, Science, 310, 1317–1321, <https://doi.org/10.1126/science.1120132>, <https://science.scienmag.org/content/310/5752/1317>, 2005.
- Stapel, J. G., Schwamborn, G., Schirrmeyer, L., Horsfield, B., and Mangelsdorf, K.: Substrate potential of last interglacial to Holocene permafrost organic matter for future microbial greenhouse gas production, Biogeosciences, 15, 1969–1985, <https://doi.org/https://doi.org/10.5194/bg-15-1969-2018>, <https://www.biogeosciences.net/15/1969/2018/>, 2018.
- 860 Stern, J. V. and Lisiecki, L. E.: Termination 1 timing in radiocarbon-dated regional benthic  $\delta^{18}\text{O}$  stacks, Paleoceanography, 29, 1127–1142, <https://doi.org/10.1002/2014PA002700>, <https://agupubs.onlinelibrary.wiley.com/doi/abs/10.1002/2014PA002700>, 2014.

- Stott, L. D., Neumann, M., and Hammond, D.: Intermediate water ventilation on the Northeastern Pacific Margin during the Late Pleistocene inferred from benthic foraminiferal  $\delta^{13}\text{C}$ , *Paleoceanography*, 15, 161–169, <https://doi.org/10.1029/1999PA000375>, <https://agupubs.onlinelibrary.wiley.com/doi/abs/10.1029/1999PA000375>, 2000.
- 875 Tarasov, P., Granoszewski, W., Bezrukova, E., Brewer, S., Nita, M., Abzaeva, A., and Oberhänsli, H.: Quantitative reconstruction of the last interglacial vegetation and climate based on the pollen record from Lake Baikal, Russia, *Climate Dynamics*, 25, 625–637, <https://doi.org/10.1007/s00382-005-0045-0>, 2005.
- Thomas, E. R., Wolff, E. W., Mulvaney, R., Steffensen, J. P., Johnsen, S. J., Arrowsmith, C., White, J. W. C., Vaughn, B., and Popp, T.: The 8.2ka event from Greenland ice cores, *Quaternary Science Reviews*, 26, 70–81, <https://doi.org/10.1016/j.quascirev.2006.07.017>, <http://www.sciencedirect.com/science/article/pii/S0277379106002393>, 2007.
- 880 Tjallingii, R., Claussen, M., Stuut, J.-B. W., Fohlmeister, J., Jahn, A., Bickert, T., Lamy, F., and Röhl, U.: Coherent high- and low-latitude control of the northwest African hydrological balance, *Nature Geoscience*, 1, 670–675, <https://doi.org/10.1038/ngeo289>, <https://www.nature.com/articles/ngeo289>, 2008.
- Tschumi, T., Joos, F., Gehlen, M., and Heinze, C.: Deep ocean ventilation, carbon isotopes, marine sedimentation and the deglacial CO<sub>2</sub> rise, *Climate of the Past*, 7, 771–800, <https://doi.org/https://doi.org/10.5194/cp-7-771-2011>, <https://www.clim-past.net/7/771/2011/cp-7-771-2011.html>, 2011.
- 885 Tzedakis, P. C., Drysdale, R. N., Margari, V., Skinner, L. C., Menviel, L., Rhodes, R. H., Taschetto, A. S., Hodell, D. A., Crowhurst, S. J., Hellstrom, J. C., Fallick, A. E., Grimalt, J. O., McManus, J. F., Martrat, B., Mokeddem, Z., Parrenin, F., Regattieri, E., Roe, K., and Zanchetta, G.: Enhanced climate instability in the North Atlantic and southern Europe during the Last Interglacial, *Nature Communications*, 9, 1–14, <https://doi.org/10.1038/s41467-018-06683-3>, <https://www.nature.com/articles/s41467-018-06683-3>, 2018.
- Venz, K. A. and Hodell, D. A.: New evidence for changes in Plio–Pleistocene deep water circulation from Southern Ocean ODP Leg 177 Site 1090, *Palaeogeography, Palaeoclimatology, Palaeoecology*, 182, 197–220, [https://doi.org/10.1016/S0031-0182\(01\)00496-5](https://doi.org/10.1016/S0031-0182(01)00496-5), <http://www.sciencedirect.com/science/article/pii/S0031018201004965>, 2002.
- 895 Venz, K. A., Hodell, D. A., Stanton, C., and Warnke, D. A.: A 1.0 Myr Record of Glacial North Atlantic Intermediate Water Variability from ODP Site 982 in the Northeast Atlantic, *Paleoceanography*, 14, 42–52, <https://doi.org/10.1029/1998PA900013>, <https://agupubs.onlinelibrary.wiley.com/doi/abs/10.1029/1998PA900013>, 1999.
- Vidal, L., Schneider, R., Marchal, O., Bickert, T., Stocker, T., and Wefer, G.: Link between the North and South Atlantic during the Heinrich events of the last glacial period, *Climate Dynamics*, 15, 909–919, <https://doi.org/10.1007/s003820050321>, <https://doi.org/10.1007/s003820050321>, 1999.
- 900 Waelbroeck, C., Duplessy, J.-C., Michel, E., Labeyrie, L., Paillard, D., and Duprat, J.: The timing of the last deglaciation in North Atlantic climate records, *Nature*, 412, 724–727, <https://doi.org/10.1038/35089060>, <https://www.nature.com/articles/35089060>, 2001.
- Waelbroeck, C., Skinner, L. C., Labeyrie, L., Duplessy, J.-C., Michel, E., Riveiros, N. V., Gherardi, J.-M., and Dewilde, F.: The timing of deglacial circulation changes in the Atlantic, *Paleoceanography*, 26, <https://doi.org/10.1029/2010PA002007>, <https://agupubs.onlinelibrary.wiley.com/doi/abs/10.1029/2010PA002007>, 2011.
- 905 Wang, L., Sarnthein, M., Erlenkeuser, H., Grimalt, J., Grootes, P., Heilig, S., Ivanova, E., Kienast, M., Pelejero, C., and Pflaumann, U.: East Asian monsoon climate during the Late Pleistocene: high-resolution sediment records from the South China Sea, *Marine Geology*, 156, 245–284, [https://doi.org/10.1016/S0025-3227\(98\)00182-0](https://doi.org/10.1016/S0025-3227(98)00182-0), <http://www.sciencedirect.com/science/article/pii/S0025322798001820>, 1999.

Wei, G.-J., Huang, C.-Y., Wang, C.-C., Lee, M.-Y., and Wei, K.-Y.: High-resolution benthic foraminifer  $\delta^{13}\text{C}$  records in the South China Sea during the last 150 ka, *Marine Geology*, 232, 227–235, <https://doi.org/10.1016/j.margeo.2006.08.005>, <http://www.sciencedirect.com/science/article/pii/S0025322706001769>, 2006.

910 Zahn, R. and Stüber, A.: Suborbital intermediate water variability inferred from paired benthic foraminiferal Cd/Ca and  $\delta^{13}\text{C}$  in the tropical West Atlantic and linking with North Atlantic climates, *Earth and Planetary Science Letters*, 200, 191–205, [https://doi.org/10.1016/S0012-821X\(02\)00613-1](https://doi.org/10.1016/S0012-821X(02)00613-1), 2002.

Zahn, R., Winn, K., and Sarnthein, M.: Benthic foraminiferal  $\delta^{13}\text{C}$  and accumulation rates of organic carbon: *Uvigerina Peregrina* group and 915 *Cibicidoides Wuellerstorfi*, *Paleoceanography*, 1, 27–42, <https://doi.org/10.1029/PA001i001p00027>, <https://agupubs.onlinelibrary.wiley.com/doi/abs/10.1029/PA001i001p00027>, 1986.

Zarriess, M. and Mackensen, A.: The tropical rainbelt and productivity changes off northwest Africa: A 31,000-year high-resolution record, *Marine Micropaleontology*, 76, 76–91, <https://doi.org/10.1016/j.marmicro.2010.06.001>, <http://www.sciencedirect.com/science/article/pii/S0377839810000587>, 2010.

920 Zarriess, M. and Mackensen, A.: Testing the impact of seasonal phytodetritus deposition on  $\delta^{13}\text{C}$  of epibenthic foraminifer *Cibicidoides wuellerstorfi*: A 31,000 year high-resolution record from the northwest African continental slope, *Paleoceanography*, 26, <https://doi.org/10.1029/2010PA001944>, <https://agupubs.onlinelibrary.wiley.com/doi/abs/10.1029/2010PA001944>, 2011.

Zarriess, M., Johnstone, H., Prange, M., Steph, S., Groeneveld, J., Mulitza, S., and Mackensen, A.: Bipolar seesaw in the northeastern tropical Atlantic during Heinrich stadials, *Geophysical Research Letters*, 38, <https://doi.org/10.1029/2010GL046070>, <https://agupubs.onlinelibrary.wiley.com/doi/abs/10.1029/2010GL046070>, 2011.

925 Zhang, J., Quay, P. D., and Wilbur, D. O.: Carbon isotope fractionation during gas-water exchange and dissolution of  $\text{CO}_2$ , *Geochimica et Cosmochimica Acta*, 59, 107–114, [https://doi.org/10.1016/0016-7037\(95\)91550-D](https://doi.org/10.1016/0016-7037(95)91550-D), <http://www.sciencedirect.com/science/article/pii/001670379591550D>, 1995.

Zhang, J., Wang, P., Li, Q., Cheng, X., Jin, H., and Zhang, S.: Western equatorial Pacific productivity and carbonate dissolution 930 over the last 550 kyr: Foraminiferal and nannofossil evidence from ODP Hole 807A, *Marine Micropaleontology*, 64, 121–140, <https://doi.org/10.1016/j.marmicro.2007.03.003>, <http://www.sciencedirect.com/science/article/pii/S0377839807000370>, 2007.